

## RESEARCH ARTICLE SUMMARY

## CORONAVIRUS

**Immunological memory to SARS-CoV-2 assessed for up to 8 months after infection**

Jennifer M. Dan\*, Jose Mateus\*, Yu Kato\*, Kathryn M. Hastie, Esther Dawen Yu, Caterina E. Faliti, Alba Grifoni, Sydney I. Ramirez, Sonya Haupt, April Frazier, Catherine Nakao, Vamseedhar Rayaprolu, Stephen A. Rawlings, Bjoern Peters, Florian Krammer, Viviana Simon, Erica Ollmann Saphire, Davey M. Smith, Daniela Weiskopf†, Alessandro Sette†, Shane Crotty†

**INTRODUCTION:** Immunological memory is the basis for durable protective immunity after infections or vaccinations. Duration of immunological memory after severe acute respiratory syndrome coronavirus 2 (SARS-CoV-2) infection and COVID-19 is unclear. Immunological memory can consist of memory B cells, antibodies, memory CD4<sup>+</sup> T cells, and/or memory CD8<sup>+</sup> T cells. Knowledge of the kinetics and interrelationships among those four types of memory in humans is limited. Understanding immune memory to SARS-CoV-2 has implications for understanding protective immunity against COVID-19 and assessing the likely future course of the COVID-19 pandemic.

**RATIONALE:** Assessing virus-specific immune memory over at least a 6-month period is likely

necessary to ascertain the durability of immune memory to SARS-CoV-2. Given the evidence that antibodies, CD4<sup>+</sup> T cells, and CD8<sup>+</sup> T cells can all participate in protective immunity to SARS-CoV-2, we measured antigen-specific antibodies, memory B cells, CD4<sup>+</sup> T cells, and CD8<sup>+</sup> T cells in the blood from subjects who recovered from COVID-19, up to 8 months after infection.

**RESULTS:** The study involved 254 samples from 188 COVID-19 cases, including 43 samples at 6 to 8 months after infection. Fifty-one subjects in the study provided longitudinal blood samples, allowing for both cross-sectional and longitudinal analyses of SARS-CoV-2-specific immune memory. Antibodies against SARS-CoV-2 spike and receptor binding domain (RBD) declined moderately over 8 months,

comparable to several other reports. Memory B cells against SARS-CoV-2 spike actually increased between 1 month and 8 months after infection. Memory CD8<sup>+</sup> T cells and memory CD4<sup>+</sup> T cells declined with an initial half-life of 3 to 5 months. This is the largest antigen-specific study to date of the four major types of immune memory for any viral infection.

Among the antibody responses, spike immunoglobulin G (IgG), RBD IgG, and neutralizing antibody titers exhibited similar kinetics. Spike IgA was still present in the large majority of subjects at 6 to 8 months after infection. Among the memory B cell responses, IgG was the dominant isotype, with a minor population of IgA memory B cells. IgM memory B cells appeared to be short-lived. CD8<sup>+</sup> T cell and CD4<sup>+</sup> T cell memory was measured for all SARS-CoV-2 proteins. Although ~70% of individuals possessed detectable CD8<sup>+</sup> T cell memory at 1 month after infection, that proportion declined to ~50% by 6 to 8 months after infection. For CD4<sup>+</sup> T cell memory, 93% of subjects had detectable SARS-CoV-2 memory at 1 month after infection, and the proportion of subjects positive for CD4<sup>+</sup> T cells (92%) remained high at 6 to 8 months after infection. SARS-CoV-2 spike-specific memory CD4<sup>+</sup> T cells with the specialized capacity to help B cells [T follicular helper (T<sub>FH</sub>) cells] were also maintained.

The different types of immune memory each had distinct kinetics, resulting in complex interrelationships between the abundance of T cell, B cell, and antibody immune memory over time. Additionally, substantially heterogeneity in memory to SARS-CoV-2 was observed.

**CONCLUSION:** Substantial immune memory is generated after COVID-19, involving all four major types of immune memory. About 95% of subjects retained immune memory at ~6 months after infection. Circulating antibody titers were not predictive of T cell memory. Thus, simple serological tests for SARS-CoV-2 antibodies do not reflect the richness and durability of immune memory to SARS-CoV-2. This work expands our understanding of immune memory in humans. These results have implications for protective immunity against SARS-CoV-2 and recurrent COVID-19. ■

The list of author affiliations is available in the full article online.

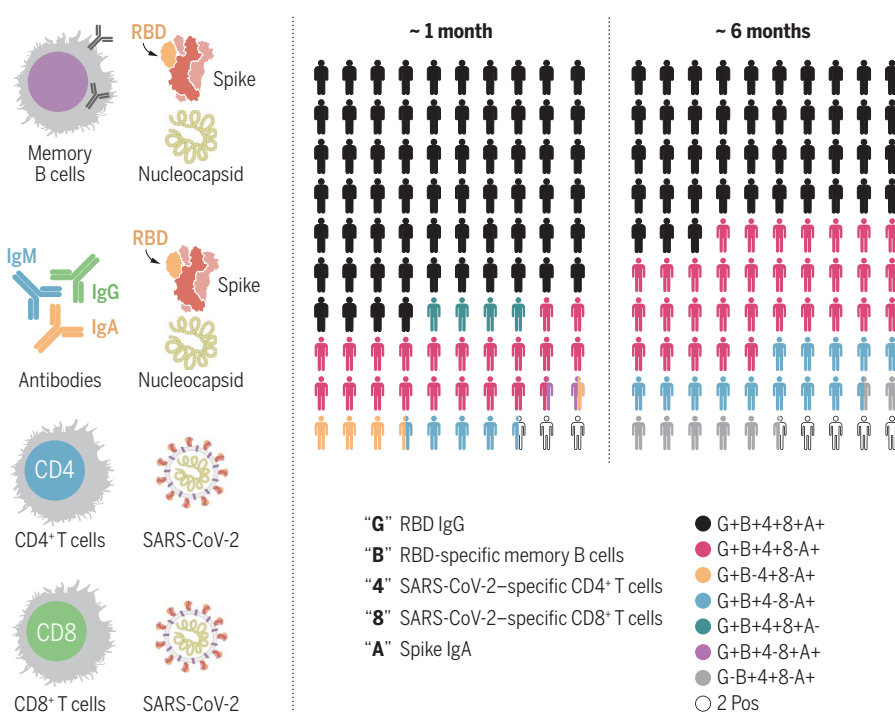
\*These authors contributed equally to this work.

†Corresponding author. Email: shane@lji.org (S.C.); alex@lji.org (A.S.); daniela@lji.org (D.W.)

This is an open-access article distributed under the terms of the Creative Commons Attribution license (<https://creativecommons.org/licenses/by/4.0/>), which permits unrestricted use, distribution, and reproduction in any medium, provided the original work is properly cited.

Cite this article as J. M. Dan et al., *Science* **371**, eabf4063 (2021). DOI: 10.1126/science.abf4063

**S** READ THE FULL ARTICLE AT  
<https://doi.org/10.1126/science.abf4063>



**Immunological memory consists of antibodies, memory B cells, memory CD8<sup>+</sup> T cells, and memory CD4<sup>+</sup> T cells.** This study examined all of the types of virus-specific immune memory against SARS-CoV-2 in COVID-19 subjects. Robust immune memory was observed in most individuals.

## RESEARCH ARTICLE

## CORONAVIRUS

**Immunological memory to SARS-CoV-2 assessed for up to 8 months after infection**

Jennifer M. Dan<sup>1,2\*</sup>, Jose Mateus<sup>1\*</sup>, Yu Kato<sup>1\*</sup>, Kathryn M. Hastie<sup>1</sup>, Esther Dawen Yu<sup>1</sup>, Caterina E. Faliti<sup>1</sup>, Alba Grifoni<sup>1</sup>, Sydney I. Ramirez<sup>1,2</sup>, Sonya Haupt<sup>1</sup>, April Frazier<sup>1</sup>, Catherine Nakao<sup>1</sup>, Vamseedhar Rayaprolu<sup>1</sup>, Stephen A. Rawlings<sup>2</sup>, Bjoern Peters<sup>1,3</sup>, Florian Krammer<sup>4</sup>, Viviana Simon<sup>4,5,6</sup>, Erica Ollmann Saphire<sup>1,2</sup>, Davey M. Smith<sup>2</sup>, Daniela Weiskopf<sup>1†</sup>, Alessandro Sette<sup>1,2†</sup>, Shane Crotty<sup>1,2†</sup>

Understanding immune memory to severe acute respiratory syndrome coronavirus 2 (SARS-CoV-2) is critical for improving diagnostics and vaccines and for assessing the likely future course of the COVID-19 pandemic. We analyzed multiple compartments of circulating immune memory to SARS-CoV-2 in 254 samples from 188 COVID-19 cases, including 43 samples at  $\geq 6$  months after infection. Immunoglobulin G (IgG) to the spike protein was relatively stable over 6+ months. Spike-specific memory B cells were more abundant at 6 months than at 1 month after symptom onset. SARS-CoV-2-specific CD4<sup>+</sup> T cells and CD8<sup>+</sup> T cells declined with a half-life of 3 to 5 months. By studying antibody, memory B cell, CD4<sup>+</sup> T cell, and CD8<sup>+</sup> T cell memory to SARS-CoV-2 in an integrated manner, we observed that each component of SARS-CoV-2 immune memory exhibited distinct kinetics.

**C**oronavirus disease 2019 (COVID-19), caused by the novel severe acute respiratory syndrome coronavirus 2 (SARS-CoV-2), is a serious disease that has resulted in widespread global morbidity and mortality. Humans make SARS-CoV-2-specific antibodies, CD4<sup>+</sup> T cells, and CD8<sup>+</sup> T cells in response to SARS-CoV-2 infection (*1–4*). Studies of acute and convalescent COVID-19 patients have observed that T cell responses are associated with reduced disease (*5–7*), suggesting that SARS-CoV-2-specific CD4<sup>+</sup> T cell and CD8<sup>+</sup> T cell responses may be important for control and resolution of primary SARS-CoV-2 infection. Ineffective innate immunity has been strongly associated with a lack of control of primary SARS-CoV-2 infection and a high risk of fatal COVID-19 (*8–12*), accompanied by innate cell immunopathology (*13–18*). Neutralizing antibodies have generally not correlated with lessened COVID-19 disease severity (*5, 19, 20*), which was also observed for Middle Eastern respiratory syndrome (MERS), caused by MERS-CoV (*21*). Instead, neutralizing antibodies are

associated with protective immunity against secondary infection with SARS-CoV-2 or SARS-CoV in nonhuman primates (*3, 22–25*). Passive transfer of neutralizing antibodies in advance of infection (mimicking preexisting conditions upon secondary exposure) effectively limits upper respiratory tract (URT) infection, lower respiratory tract (lung) infection, and symptomatic disease in animal models (*26–28*). Passive transfer of neutralizing antibodies provided after initiation of infection in humans has had more limited effects on COVID-19 (*29, 30*), consistent with a substantial role for T cells in control and clearance of an ongoing SARS-CoV-2 infection. Thus, studying antibody, memory B cell, CD4<sup>+</sup> T cell, and CD8<sup>+</sup> T cell memory to SARS-CoV-2 in an integrated manner is likely important for understanding the durability of protective immunity against COVID-19 generated by primary SARS-CoV-2 infection (*1, 19, 31*).

Whereas sterilizing immunity against viruses can only be accomplished by high-titer neutralizing antibodies, successful protection against clinical disease or death can be accomplished by several other immune memory scenarios. Possible mechanisms of immunological protection can vary according to the relative kinetics of the immune memory responses and infection. For example, clinical hepatitis after hepatitis B virus (HBV) infection is prevented by vaccine-elicited immune memory even in the absence of circulating antibodies, because of the relatively slow course of HBV disease (*32, 33*). The relatively slow course of severe COVID-19 in humans [median 19 days post-symptom onset (PSO) for fatal cases (*34*)] suggests that protective

immunity against symptomatic or severe secondary COVID-19 may involve memory compartments such as circulating memory T cells and memory B cells (which can take several days to reactivate and generate recall T cell responses and/or anamnestic antibody responses) (*19, 21, 31*).

Immune memory, from either primary infection or immunization, is the source of protective immunity from a subsequent infection (*35–37*). Thus, COVID-19 vaccine development relies on immunological memory (*1, 3*). Despite intensive study, the kinetics, duration, and evolution of immune memory in humans to infection or immunization are not in general predictable on the basis of the initial effector phase, and immune responses at short time points after resolution of infection are not very predictive of long-term memory (*38–40*). Thus, assessing responses over an interval of 6 months or more is usually required to ascertain the durability of immune memory.

A thorough understanding of immune memory to SARS-CoV-2 requires evaluation of its various components, including B cells, CD8<sup>+</sup> T cells, and CD4<sup>+</sup> T cells, as these different cell types may have immune memory kinetics that are relatively independent of each other. Understanding the complexities of immune memory to SARS-CoV-2 is key to gaining insights into the likelihood of durability of protective immunity against reinfection with SARS-CoV-2 and secondary COVID-19 disease. In this study, we assessed immune memory of all three branches of adaptive immunity (CD4<sup>+</sup> T cell, CD8<sup>+</sup> T cell, and humoral immunity) in a predominantly cross-sectional study of 188 recovered COVID-19 cases, extending up to 8 months after infection. The findings have implications for immunity against secondary COVID-19, and thus the potential future course of the pandemic (*41, 42*).

**COVID-19 cohort**

We recruited 188 individuals with COVID-19 for this study. Subjects (80 male, 108 female) represented a range of asymptomatic, mild, moderate, and severe COVID-19 cases (Table 1) and were recruited from multiple sites throughout the United States. The majority of subjects were from California or New York. Most subjects had a “mild” case of COVID-19, not requiring hospitalization. Ninety-three percent of subjects were never hospitalized for COVID-19; 7% of subjects were hospitalized, some of whom required intensive care unit (ICU) care (Table 1). This case severity distribution was consistent with the general distribution of symptomatic disease severity among COVID-19 cases in the United States. The study primarily consisted of symptomatic disease cases (97%, Table 1), owing to the nature of the study recruitment design. Subject ages ranged from 19 to 81 years old (Table 1). Most subjects provided a blood

\*Center for Infectious Disease and Vaccine Research, La Jolla Institute for Immunology (LJI), La Jolla, CA 92037, USA.

†Department of Medicine, Division of Infectious Diseases and Global Public Health, University of California, San Diego (UCSD), La Jolla, CA 92037, USA. <sup>2</sup>Department of Medicine, University of California, San Diego (UCSD), La Jolla, CA 92037, USA. <sup>3</sup>Department of Microbiology, Icahn School of Medicine at Mount Sinai, New York, NY 10029, USA.

<sup>4</sup>Division of Infectious Diseases, Department of Medicine, Icahn School of Medicine at Mount Sinai, New York, NY 10029, USA. <sup>5</sup>The Global Health and Emerging Pathogens Institute, Icahn School of Medicine at Mount Sinai, New York, NY 10029, USA.

\*These authors contributed equally to this work.

†Corresponding author. Email: shane@lji.org (S.C.); alex@lji.org (A.S.); daniela@lji.org (D.W.)

**Table 1.** Participant characteristics.

	COVID-19 (n = 188)
Age (years)	19 to 81 (median = 40, IQR* = 18.75)
Gender	
Male (%)	43% (80/188)
Female (%)	57% (108/188)
Race	
African American or Black (%)	3% (5/188)
Alaskan Native or American Indian (%)	1% (1/188)
Asian (%)	7% (14/188)
Native Hawaiian or Pacific Islander (%)	0% (0/188)
Multiracial (%)	1% (2/188)
Other (%)	1% (1/188)
Unknown (%)	10% (19/188)
White (%)	78% (146/188)
Ethnicity	
Hispanic or Latino (%)	15% (28/188)
Non-Hispanic (%)	80% (150/188)
Unknown (%)	5% (10/188)
Hospitalization status	
Never hospitalized (%)	93% (174/188)
Hospitalized (%)	7% (13/188)
Unknown if hospitalized (%)	1% (1/188)
Sample collection dates	March–October 2020
SARS-CoV-2 PCR positivity	
Positive	77% (145/188)
Negative	1% (2/188)
Not performed	20% (37/188)
Unknown	2% (4/188)
Peak disease severity (%) [Female (F), Male (M)]	
Asymptomatic (score 1)	2% (4/188) (2F, 2M)
Mild (nonhospitalized; score 2–3)	90% (170/188) (100F, 70M)
Moderate (hospitalized; score 4–5)	3% (6/188) (3F, 3M)
Severe (hospitalized; Score 6+)	4% (7/188) (3F, 4M)
Unknown	1% (1/188) (0F, 1M)
Days post-symptom onset at collection; n = 254	6–240 (median 88, IQR 97.75)
Blood collection frequency	
Multiple time point	27% (51/188)
Donors (two to four times)	
Single-time point donors	73% (137/188)

\*IQR, interquartile range.

sample at a single time point, between 6 and 240 days PSO (Table 1), with 43 samples at  $\geq 6$  months PSO (178 days or longer). Additionally, 51 subjects in the study provided longitudinal blood samples over a duration of several months (two to four time points; Table 1), allowing for longitudinal assessment of immune memory in a subset of the cohort.

#### SARS-CoV-2 circulating antibodies over time

The vast majority of SARS-CoV-2-infected individuals seroconvert, at least for a duration of months (1, 2, 4, 43–45). Seroconversion rates range from 91 to 99% in large studies (44, 45).

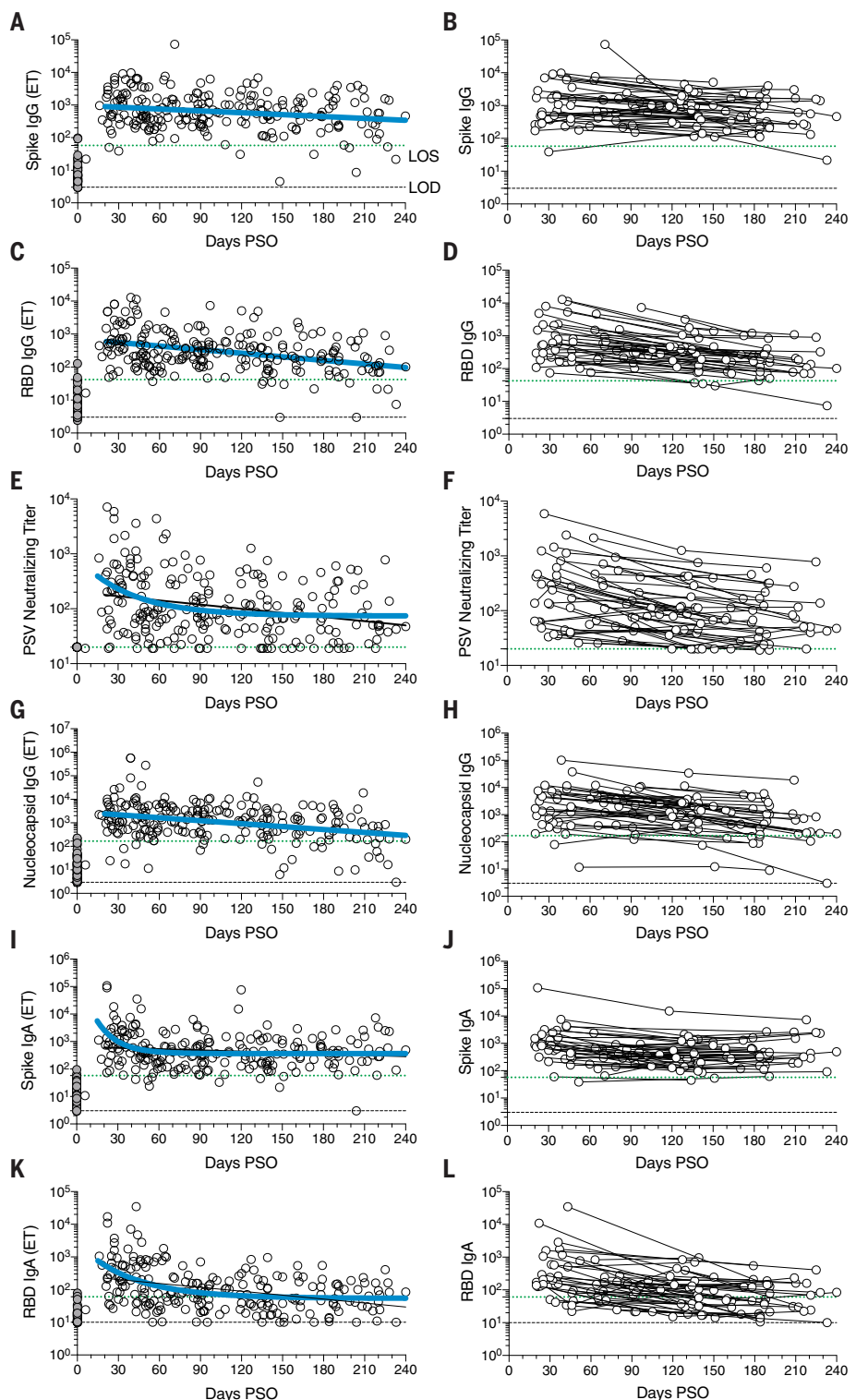
Durability assessments of circulating antibody titers in Fig. 1 were based on data  $\geq 20$  days PSO, with the plot of the best-fitting curve fit model shown in blue (see materials and methods). SARS-CoV-2 spike immunoglobulin G (IgG) endpoint enzyme-linked immunosorbent assay (ELISA) titers in plasma were measured for all subjects of this cohort (Fig. 1, A and B). Spike receptor binding domain (RBD) IgG was also measured (Fig. 1, C and D), as RBD is the target of most neutralizing antibodies against SARS-CoV-2 (4, 27, 46, 47). SARS-CoV-2 pseudovirus (PSV)-neutralizing antibody titers were measured in all subjects

(Fig. 1, E and F). Nucleocapsid (N) IgG endpoint ELISA titers were also measured for all subjects (Fig. 1, G and H), as nucleocapsid is a common antigen in commercial SARS-CoV-2 serological test kits.

SARS-CoV-2 spike IgG titers were relatively stable from 20 to 240 days PSO, when assessing all COVID-19 subjects by cross-sectional analysis (half-life  $t_{1/2} = 140$  days, Fig. 1A). Spike IgG titers were heterogeneous among subjects (range 5 to 73,071; median 575), as has been widely observed (45, 47). This gave a wide confidence interval (CI) for the spike IgG  $t_{1/2}$  (95% CI: 89 to 325 days). Although the antibody responses may have more complex underlying decay kinetics, the best fit curve was a continuous decay, likely related to heterogeneity between individuals. SARS-CoV-2 nucleocapsid IgG kinetics were similar to those of spike IgG over 8 months ( $t_{1/2}$  68 days; 95% CI: 50 to 106 days, Fig. 1G). As a complementary approach, using paired samples from the subset of subjects who donated at two or more time points, the calculated spike IgG titer average  $t_{1/2}$  was 103 days, (95% CI: 66 to 235 days; Fig. 1B) and the nucleocapsid IgG titer average  $t_{1/2}$  was 68 days, (95% CI: 55 to 90 days; Fig. 1H). The percentage of subjects seropositive for spike IgG at 1 month PSO (20 to 50 days) was 98% (54 out of 55). The percentage of subjects seropositive for spike IgG at 6 to 8 months PSO ( $\geq 178$  days) was 90% (36 out of 40).

Cross-sectional analysis of SARS-CoV-2 RBD IgG titers from 20 to 240 days PSO gave an estimated  $t_{1/2}$  of 83 days (95% CI: 62 to 126 days; Fig. 1C). As a complementary approach, we again used paired samples, which gave an average  $t_{1/2}$  of 69 days (95% CI: 58 to 87 days; Fig. 1D). The percentage of subjects seropositive for RBD IgG at 6 to 8 months PSO was 88% (35 out of 40). Thus, RBD IgG titer maintenance largely matched that of spike IgG. SARS-CoV-2 PSV neutralization titers in the full cohort largely matched the results of SARS-CoV-2 RBD IgG ELISA binding titers (Fig. 1, E and F). A one-phase decay model was the best fit ( $P = 0.015$ , F test; initial decay  $t_{1/2}$  27 days, followed by an extended plateau phase, Fig. 1E), whereas a continuous decay fit gave an estimated  $t_{1/2}$  of 114 days (Fig. 1E, black line). Paired time points analysis of the PSV neutralization titers gave an estimated  $t_{1/2}$  of 90 days, (95% CI: 70 to 125 days; Fig. 1F). The percentage of subjects seropositive for SARS-CoV-2-neutralizing antibodies (titer  $\geq 20$ ) at 6 to 8 months PSO was 90% (36 out of 40). Notably, even low circulating neutralizing antibody titers ( $\geq 1:20$ ) were associated with a substantial degree of protection against COVID-19 in nonhuman primates (24, 48). Thus, modest amounts of circulating SARS-CoV-2 neutralizing antibodies are of biological interest in humans.

**Fig. 1. Circulating antibodies to SARS-CoV-2 over time.** (A) Cross-sectional spike IgG from COVID-19 subject plasma samples ( $n = 228$ ). Continuous decay preferred model for best fit curve,  $t_{1/2} = 140$  days; 95% CI: 89 to 325 days.  $R = -0.23$ ,  $p = 0.0006$ . (B) Longitudinal spike IgG ( $n = 51$ ), average  $t_{1/2} = 103$  days; 95% CI: 65 to 235 days. (C) Cross-sectional RBD IgG. Continuous decay preferred model for best fit curve,  $t_{1/2} = 83$  days; 95% CI: 62 to 126 days.  $R = -0.36$ ,  $p < 0.0001$ . (D) Longitudinal RBD IgG, average  $t_{1/2} = 69$  days; 95% CI: 58 to 87 days. (E) Cross-sectional SARS-CoV-2 PSV-neutralizing titers. One-phase decay (blue line) preferred model for best fit curve, initial  $t_{1/2} = 27$  days; 95% CI: 11 to 157 days.  $R = -0.32$ . Continuous decay fit line shown as black line. (F) Longitudinal PSV-neutralizing titers of SARS-CoV-2-infected subjects, average  $t_{1/2} = 90$  days; 95% CI: 70 to 125 days. (G) Cross-sectional nucleocapsid IgG. Continuous decay preferred model for best fit curve,  $t_{1/2} = 68$  days; 95% CI: 50 to 106 days.  $R = -0.34$ ,  $p < 0.0001$ . (H) Longitudinal nucleocapsid IgG, average  $t_{1/2} = 68$  days; 95% CI: 55 to 90 days. (I) Cross-sectional spike IgA titers. One-phase decay (blue line) preferred model for best fit curve, initial  $t_{1/2} = 11$  days; 95% CI: 5 to 25 days.  $R = -0.30$ . Continuous decay fit shown as black line. (J) Longitudinal spike IgA,  $t_{1/2} = 210$  days, 95% CI 126 to 627 days. (K) Cross-sectional RBD IgA. One-phase decay (blue line) preferred model for best fit curve, initial  $t_{1/2} = 27$  days; 95% CI: 15 to 59 days.  $R = -0.45$ . Continuous decay line fit shown in black. (L) Longitudinal RBD IgA, average  $t_{1/2} = 74$  days; 95% CI: 56 to 107 days. For cross-sectional analyses, SARS-CoV-2-infected subjects (white circles,  $n = 238$ ) and unexposed subjects (gray circles,  $n = 51$ ). For longitudinal samples, SARS-CoV-2 subjects ( $n = 51$ ). The dotted black line indicates limit of detection (LOD). The dotted green line indicates limit of sensitivity (LOS) above uninfected controls. Unexposed subjects are depicted in gray, COVID subjects in white. Log data analyzed in all cases. Thick blue line represents best fit curve. When two fit curves are shown, the thin black line represents the alternative fit curve.



SARS-CoV-2 spike IgA (Fig. 1, I and J) and RBD IgA (Fig. 1, K and L) titers were also assessed. Paired time points analysis of spike IgA titers yielded an estimated  $t_{1/2}$  of 210 days (95% CI 126 to 703 days, Fig. 1J). Cross-sectional analysis of spike IgA fit a short one-phase decay model with an extended plateau phase (initial  $t_{1/2}$  of 14 days, Fig. 1I). Circulating RBD IgA had

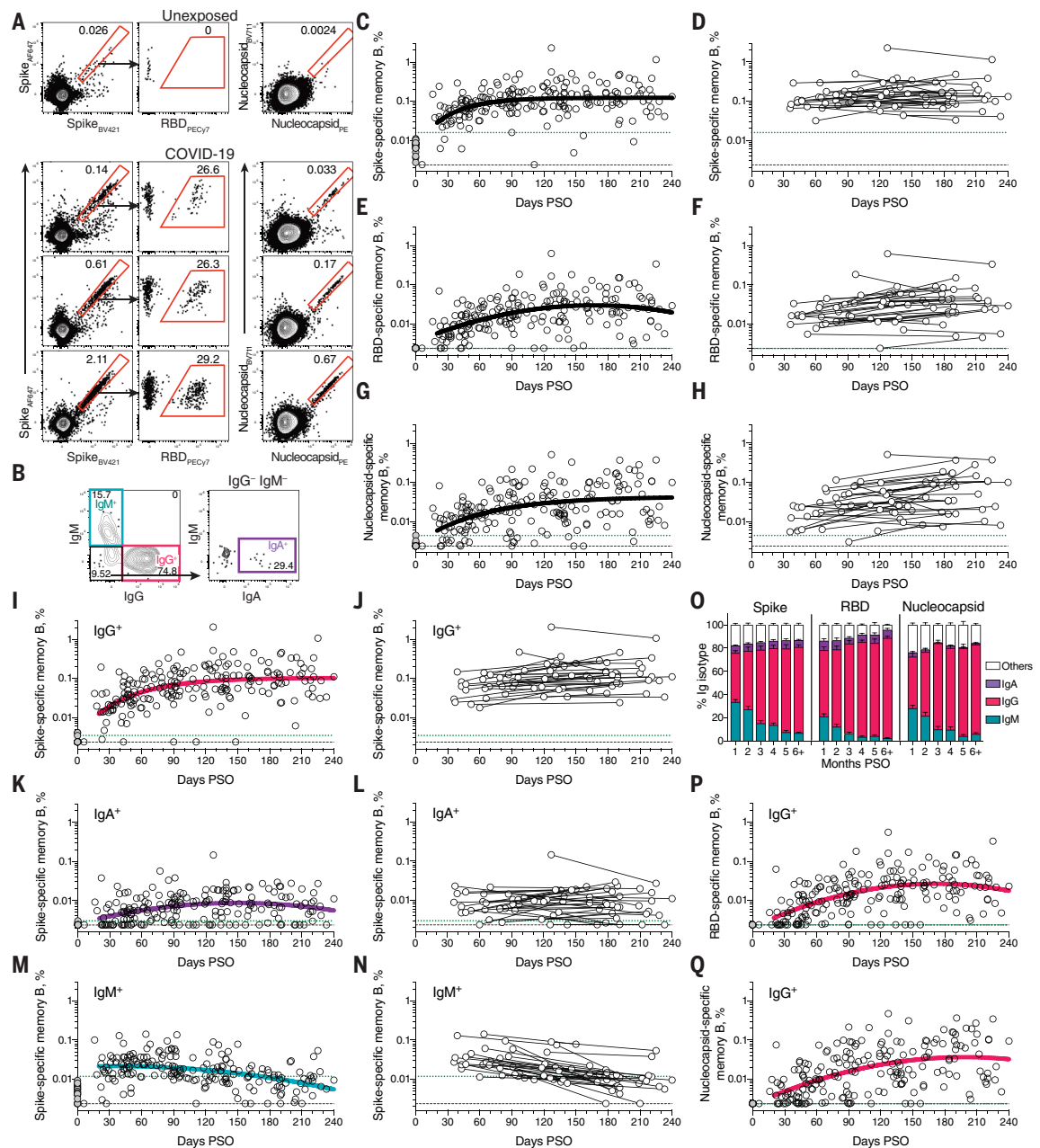
an estimated initial  $t_{1/2}$  of 27 days, decaying by ~90 days in most COVID-19 cases to levels indistinguishable from those of uninfected controls (Fig. 1K), consistent with observations 3 months PSO (44, 49). By paired sample analysis, long-lasting RBD IgA was made in some subjects, but often near the limit of sensitivity (LOS) (Fig. 1L).

### SARS-CoV-2 memory B cells

To identify SARS-CoV-2-specific memory B cells, we used fluorescently labeled multimerized probes to detect B cells specific to spike, RBD, and nucleocapsid (Fig. 2A and fig. S1). Antigen-binding memory B cells (defined as IgD<sup>-</sup> and/or CD27<sup>+</sup>) were further distinguished according to surface

**Fig. 2. Kinetics of SARS-CoV-2 memory B cell responses.**

**(A)** Example flow cytometry plots showing staining patterns of SARS-CoV-2 antigen probes on memory B cells (see fig. S1 for gating). One unexposed donor and three convalescent COVID-19 subjects are shown. Numbers indicate percentages. **(B)** Gating strategies to define IgM<sup>+</sup>, IgG<sup>+</sup>, or IgA<sup>+</sup> SARS-CoV-2 spike-specific memory B cells. The same gating strategies were used for RBD- or nucleocapsid-specific B cells. **(C)** Cross-sectional analysis of frequency (percentage of CD19<sup>+</sup> CD20<sup>+</sup> B cells) of SARS-CoV-2 spike-specific total (IgG<sup>+</sup>, IgM<sup>+</sup>, or IgA<sup>+</sup>) memory B cells. Pseudo-first-order kinetic model for best fit curve ( $R = 0.38$ ). **(D)** Longitudinal analysis of SARS-CoV-2 spike-specific memory B cells. **(E)** Cross-sectional analysis of SARS-CoV-2 RBD-specific total (IgG<sup>+</sup>, IgM<sup>+</sup>, or IgA<sup>+</sup>) memory B cells. Second-order polynomial model for best fit curve ( $R = 0.46$ ). **(F)** Longitudinal analysis of SARS-CoV-2 RBD-specific memory B cells. **(G)** Cross-sectional analysis of SARS-CoV-2 nucleocapsid-specific total (IgG<sup>+</sup>, IgM<sup>+</sup>, or IgA<sup>+</sup>) memory B cells. Pseudo-first-order kinetic model for best fit curve ( $R = 0.44$ ). **(H)** Longitudinal analysis of IgG<sup>+</sup> SARS-CoV-2 nucleocapsid-specific memory B cells. **(I)** Cross-sectional analysis of SARS-CoV-2 spike-specific IgG<sup>+</sup> memory B cells. Pseudo-first-order kinetic model for best fit curve ( $R = 0.49$ ). **(J)** Longitudinal analysis of SARS-CoV-2 spike-specific IgG<sup>+</sup> memory B cells. **(K)** Cross-sectional analysis of SARS-CoV-2 spike-specific IgA<sup>+</sup> memory B cells. Second-order polynomial model for best fit curve ( $|R| = 0.32$ ). **(L)** Longitudinal analysis of SARS-CoV-2 spike-specific IgA<sup>+</sup> memory B cells. **(M)** Cross-sectional analysis of SARS-CoV-2 spike-specific IgM<sup>+</sup> memory B cells. Second-order polynomial model for best fit curve ( $|R| = 0.41$ ).



**(N)** Longitudinal analysis of SARS-CoV-2 spike-specific IgM<sup>+</sup> memory B cells.

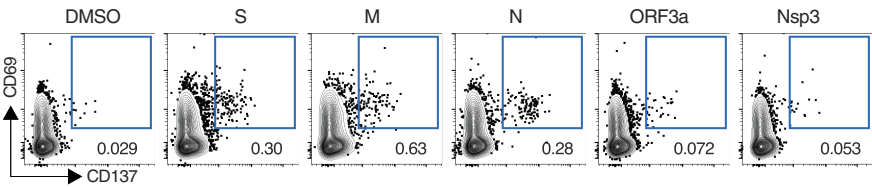
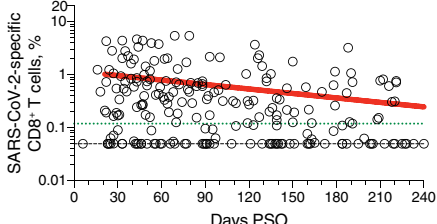
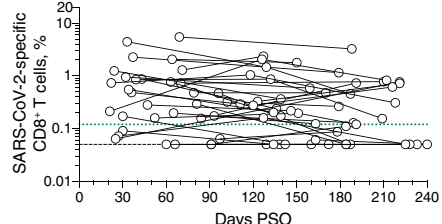
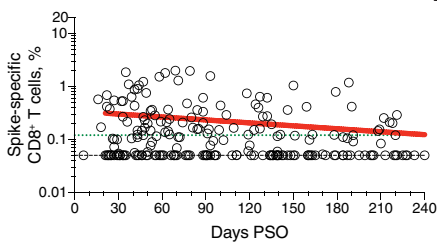
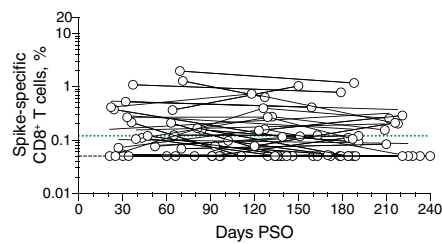
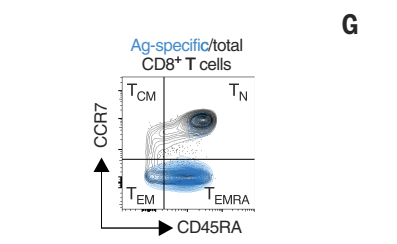
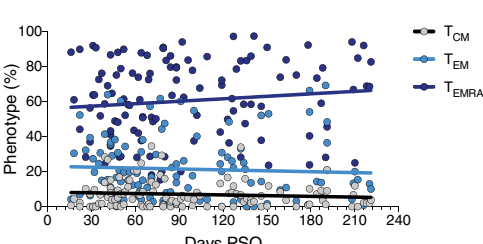
**(O)** Fraction of SARS-CoV-2 antigen-specific memory B cells that belong to indicated Ig isotypes at 1 to 8 months PSO. Mean  $\pm$  SEM. **(P)** Cross-sectional analysis of SARS-CoV-2 RBD-specific IgG<sup>+</sup> memory B cells. Second-order polynomial model for best fit curve ( $|R| = 0.51$ ). **(Q)** Cross-sectional analysis of SARS-CoV-2 nucleocapsid-specific IgG<sup>+</sup> memory B cells. Second-order polynomial model for best fit curve ( $|R| = 0.51$ ).  $n = 20$  unexposed subjects (gray circles) and  $n = 160$  COVID-19 subjects ( $n = 197$  data points, white circles) for cross-sectional analysis.  $n = 36$  COVID-19 subjects ( $n = 73$  data points, white circles) for longitudinal analysis. The dotted black line indicates LOD. The dotted green line indicates LOS.

Ig isotypes: IgM, IgG, or IgA (Fig. 2B and fig. S1).

Cross-sectional analysis of COVID-19 subjects revealed that frequencies of SARS-CoV-2 spike-specific memory B cells increased over the first

~120 days PSO and then plateaued (pseudo-first-order model for best fit curve,  $R = 0.38$ ; better fit than second-order polynomial model by Akaike's information criterion; Fig. 2C and fig. S2A). Spike-specific memory B cell fre-

quencies increased from the first time point (36 to 163 days) to the second time point (111 to 240 days) in paired samples from 24 of 36 longitudinally tracked donors (Fig. 2D). Spike-specific memory B cells in SARS-CoV-2-unexposed

**A****B****C****D****E****F****G**

**Fig. 3. SARS-CoV-2 circulating memory CD8<sup>+</sup> T cells.** (A) Representative flow cytometry plots of SARS-CoV-2-specific CD8<sup>+</sup> T cells (CD69<sup>+</sup> CD137<sup>+</sup>; see fig. S3 for gating) after overnight stimulation with S, N, M, ORF3a, or nsp3 peptide pools, compared to negative control (DMSO). (B) Cross-sectional analysis of frequency (percentage of CD8<sup>+</sup> T cells) of total SARS-CoV-2-specific CD8<sup>+</sup> T cells. Continuous decay preferred fit model,  $t_{1/2} = 125$  days.  $R = -0.24$ ,  $p = 0.0003$ . (C) Longitudinal analysis of total SARS-CoV-2-specific CD8<sup>+</sup> T cells in paired samples. (D) Cross-sectional analysis of spike-specific CD8<sup>+</sup> T cells. Linear decay preferred model,  $t_{1/2} = 225$  days.  $R = -0.18$ ,  $p = 0.007$ . (E) Longitudinal analysis of spike-specific CD8<sup>+</sup> T cells in paired samples. (F and G) Distribution of central memory (T<sub>CM</sub>), effector memory (T<sub>EM</sub>), and terminally differentiated effector memory cells (T<sub>EMRA</sub>) among total SARS-CoV-2-specific CD8<sup>+</sup> T cells.  $n = 169$  COVID-19 subjects ( $n = 215$  data points, white circles) for cross-sectional analysis.  $n = 37$  COVID-19 subjects ( $n = 83$  data points, white circles) for longitudinal analysis. The dotted black line indicates LOD. The dotted green line indicates LOS.

subjects were rare (median 0.007%; Fig. 2, A and C).

RBD-specific memory B cells displayed similar kinetics to spike-specific memory B cells. RBD-specific memory B cells were undetectable in SARS-CoV-2-unexposed subjects (Fig. 2E and fig. S2C), as expected. RBD-specific memory B cells appeared as early as 16 days PSO, and the frequency steadily increased in the following 4 to 5 months (Fig. 2E and fig. S2, B and C). Twenty-nine of 36 longitudinally tracked individuals had higher frequencies of RBD-specific memory B cells at the later time point (Fig. 2F), again showing an in-

crease in SARS-CoV-2-specific memory B cells several months after infection. About 10 to 30% of spike-specific memory B cells from SARS-CoV-2 convalescent donors were specific for the RBD domain (Fig. 2A and fig. S2B).

SARS-CoV-2 nucleocapsid-specific memory B cells were also detected after SARS-CoV-2 infection (Fig. 2A). Similar to spike- and RBD-specific memory B cells, nucleocapsid-specific memory B cell frequency steadily increased during the first ~4 to 5 months PSO (Fig. 2, G and H, and fig. S2D). Antibody affinity maturation could potentially explain the increased frequencies of SARS-CoV-2-specific memory

B cells detected by the antigen probes. However, geometric mean fluorescent intensity (MFI) of probe binding was stable over time (fig. S2, I and J), not supporting an affinity maturation explanation for the increased memory B cell frequencies.

Representation of Ig isotypes among the SARS-CoV-2 spike-specific memory B cell population shifted with time (Fig. 2, I to O). During the earliest phase of memory (20 to 60 days PSO), IgM<sup>+</sup> and IgG<sup>+</sup> isotypes were similarly represented (Fig. 2O), but IgM<sup>+</sup> memory B cells then declined (Fig. 2, M to O), and IgG<sup>+</sup> spike-specific memory B cells then dominated by 6 months PSO (Fig. 2O). IgA<sup>+</sup> spike-specific memory B cells were detected as a small fraction of the total spike-specific memory B cells (~5%, Fig. 2O). IgG<sup>+</sup> spike-specific memory B cell frequency increased, whereas IgA<sup>+</sup> frequency was low and stable over the 8-month period (Fig. 2, I to L). Similar patterns of increasing IgG<sup>+</sup> memory, short-lived IgM<sup>+</sup> memory, and stable IgA<sup>+</sup> memory were observed for RBD- and nucleocapsid-specific memory B cells over the 8-month period (Fig. 2, O to Q, and fig. S2, E to H).

There is limited knowledge of memory B cell kinetics following primary acute viral infection in humans. A recently published SARS-CoV-2 study found RBD-specific memory B cells up to ~90 days PSO, with increasing frequencies (and a low frequency of IgA<sup>+</sup> cells) (50), consistent with observations reported here. For other acute infectious diseases, we are not currently aware of other cross-sectional or longitudinal analyses of antigen-specific memory B cells by flow cytometry covering a 6+ month window after infection, except for four individuals with Ebola (51) and two individuals studied after yellow fever virus immunization (52) (we exclude influenza vaccines for comparison here, because people have numerous exposures and complex immune history to influenza). In the yellow fever study, short-lived IgM<sup>+</sup> memory and longer-lasting isotype-switched memory B cells were observed in the two individuals. Overall, on the basis of the observations here, development of B cell memory to SARS-CoV-2 was robust and is likely long-lasting.

### SARS-CoV-2 memory CD8<sup>+</sup> T cells

SARS-CoV-2 memory CD8<sup>+</sup> T cells were measured in 169 COVID-19 subjects using a series of 23 peptide pools covering the entirety of the SARS-CoV-2 ORFeome (2, 5). The most commonly recognized open reading frames (ORFs) were spike, membrane (M), nucleocapsid, and ORF3a (CD69<sup>+</sup> CD137<sup>+</sup>; Fig. 3A and fig. S3, A and B), consistent with our previous study (2). The percentage of subjects with detectable circulating SARS-CoV-2 memory CD8<sup>+</sup> T cells at 1 month PSO (20 to 50 days) was 70% (40 out of 57, Fig. 3B).

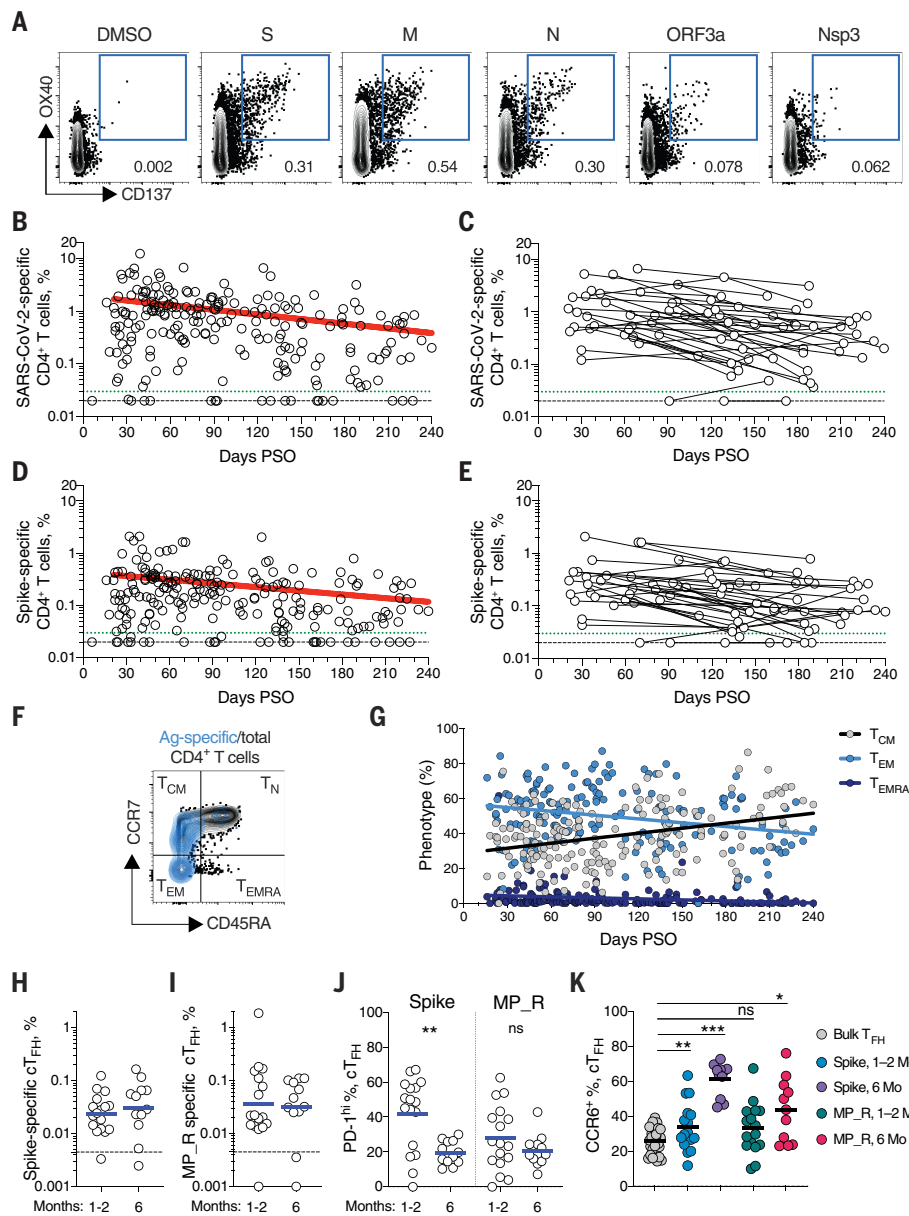


**Fig. 4. SARS-CoV-2 circulating memory CD4<sup>+</sup> T cells.** (A) Representative flow cytometry plots of SARS-CoV-2-specific CD4<sup>+</sup> T cells (CD137<sup>+</sup> OX40<sup>+</sup>; see fig. S4 for gating) after overnight stimulation with S, N, M, ORF3a, or nsp3 peptide pools, compared to negative control (DMSO). (B) Cross-sectional analysis of frequency (percentage of CD4<sup>+</sup> T cells) of total SARS-CoV-2-specific CD4<sup>+</sup> T cells. Continuous decay preferred fit model,  $t_{1/2} = 94$  days.  $R = -0.29$ ,  $p < 0.0001$ . (C) Longitudinal analysis of total SARS-CoV-2-specific CD4<sup>+</sup> T cells in paired samples from the same subjects. (D) Cross-sectional analysis of spike-specific CD4<sup>+</sup> T cells. Linear decay preferred model,  $t_{1/2} = 139$  days.  $R = -0.26$ ,  $p < 0.0001$ . (E) Longitudinal analysis of spike-specific CD4<sup>+</sup> T cells in paired samples from the same subjects. (F and G) Distribution of central memory (T<sub>CM</sub>), effector memory (T<sub>EM</sub>), and terminally differentiated effector memory cells (T<sub>EMRA</sub>) among total SARS-CoV-2-specific CD4<sup>+</sup> T cells. (H and I) Quantitation of SARS-CoV-2-specific circulating T follicular helper (cT<sub>FH</sub>) cells (surface CD40L<sup>+</sup> OX40<sup>+</sup>, as percentage of CD4<sup>+</sup> T cells; see fig. S5 for gating) after overnight stimulation with (H) spike (S) or (I) MP\_R peptide pools. (J) PD-1<sup>hi</sup> SARS-CoV-2-specific T<sub>FH</sub> at 1 to 2 months (mo) and 6 mo PSO. (K) CCR6<sup>+</sup> SARS-CoV-2-specific cT<sub>FH</sub> in comparison to bulk cT<sub>FH</sub> cells in blood. For (A) to (E),  $n = 169$  COVID-19 subjects ( $n = 215$  data points, white circles) for cross-sectional analysis,  $n = 37$  COVID-19 subjects ( $n = 83$  data points, white circles) for longitudinal analysis. The dotted black line indicates limit of detection. The dotted green line indicates LOS. For (H) to (J),  $n = 29$  COVID-19 subject samples (white circles),  $n = 17$  COVID-19 subjects at 1 to 2 mo,  $n = 12$  COVID-19 subjects at 6 mo. The dotted black line indicates LOD. Statistics by (J) Mann-Whitney U test and (K) Wilcoxon signed-rank test. \* $p < 0.05$ , \*\* $p < 0.01$ , \*\*\* $p < 0.001$ . ns, not statistically significant.

The proportion of subjects positive for SARS-CoV-2 memory CD8<sup>+</sup> T cells at  $\geq 6$  months PSO was 50% (18 out of 36). This could potentially underestimate CD8<sup>+</sup> T cell memory, as 15-mer peptides can be suboptimal for detection of some antigen-specific CD8<sup>+</sup> T cells (53); however, pools of predicted SARS-CoV-2 class I epitope of optimal size also detected virus-specific CD8<sup>+</sup> T cells in ~70% of individuals 1 to 2 months PSO, indicating consistency between the two experimental approaches (2).

SARS-CoV-2 memory CD8<sup>+</sup> T cells declined with an apparent  $t_{1/2}$  of 125 days in the full cohort (Fig. 3B) and  $t_{1/2}$  190 days among 29 paired samples (Fig. 3C). Spike-specific memory CD8<sup>+</sup> T cells exhibited similar kinetics to the overall SARS-CoV-2-specific memory CD8<sup>+</sup> T cells ( $t_{1/2}$  225 days for the full cohort and 185 days among paired samples; Fig. 3, D and E, respectively). Phenotypic markers indicated that the majority of SARS-CoV-2-specific memory CD8<sup>+</sup> T cells were terminally differentiated effector memory cells (T<sub>EMRA</sub>) (54), with small populations of central memory (T<sub>CM</sub>) and effector memory (T<sub>EM</sub>) (Fig. 3, F and G). In the context of influenza, CD8<sup>+</sup> T<sub>EMRA</sub> cells were associated with protection against severe disease in humans (55). The memory CD8<sup>+</sup> T cell half-lives observed here were comparable to the 123 days  $t_{1/2}$  observed for memory CD8<sup>+</sup> T cells after yellow fever immunization (56). Thus, the kinetics of circulating SARS-CoV-2-specific CD8<sup>+</sup> T cell were consistent with what has been reported for another virus that causes acute infections in humans.

### SARS-CoV-2 memory CD4<sup>+</sup> T cells

SARS-CoV-2 memory CD4<sup>+</sup> T cells were identified in 169 subjects using the same series of 23 peptide pools covering the SARS-CoV-2 ORFeome (2, 5). The most commonly recognized ORFs were spike, M, nucleocapsid, ORF3a, and nsp3 (CD137<sup>+</sup> OX40<sup>+</sup>; Fig. 4A and fig. S4, A and B), consistent with our previous study (2). Circulating SARS-CoV-2 memory CD4<sup>+</sup> T cell responses were quite robust (Fig. 4B); 42% (24 out of 57) of COVID-19 cases at 1 month PSO had  $>10\%$  SARS-CoV-2-specific CD4<sup>+</sup> T cells. SARS-CoV-2 memory CD4<sup>+</sup> T cells declined with an apparent  $t_{1/2}$  of 94 days in the full cohort (Fig. 4B) and 64 days among 36 paired samples (Fig. 4C). The percentage of subjects with detectable circulating SARS-CoV-2 memory CD4<sup>+</sup> T cells at 1 month PSO (20 to 50 days) was 93% (53 out of 57, Fig. 4B). The proportion of subjects positive for SARS-CoV-2 memory CD4<sup>+</sup> T cells at  $\geq 6$  months PSO was 92% (33 out of 36).

Spike-specific and M-specific memory CD4<sup>+</sup> T cells exhibited similar kinetics to the overall SARS-CoV-2-specific memory CD4<sup>+</sup> T cells (whole cohort  $t_{1/2}$  of 139 days and 153 days, respectively; Fig. 4, D and E, and fig. S4D). A plurality of the SARS-CoV-2 memory CD4<sup>+</sup>

T cells present at  $\geq 6$  months PSO had a T<sub>CM</sub> phenotype (Fig. 4F).

T follicular helper (T<sub>FH</sub>) cells are the specialized subset of CD4<sup>+</sup> T cells required for B cell help (57) and are therefore critical for the generation of neutralizing antibodies and long-lived humoral immunity in most contexts. Thus, we examined circulating T<sub>FH</sub> (cT<sub>FH</sub>) memory CD4<sup>+</sup> T cells, with particular interest in spike-specific memory cT<sub>FH</sub> cells, owing to the importance of antibody responses against spike. Memory cT<sub>FH</sub> cells specific for predicted epitopes across the remainder of the SARS-CoV-2 genome were also measured, using the MP\_R megapool. Memory cT<sub>FH</sub> cells specific for SARS-CoV-2 spike and MP\_R were detected in the majority of COVID-19 cases at early time points (16 out of 17; Fig. 4, H and I, and fig. S5, A to D). cT<sub>FH</sub> memory appeared to be stable, with almost all subjects positive for spike and MP\_R memory cT<sub>FH</sub> cells at 6 months PSO (11 out of 12 and 10 out of 12, respectively; Fig. 4, H and I). Recently activated cT<sub>FH</sub> cells are PD-1<sup>hi</sup> (57). Consistent with conversion to resting memory cT<sub>FH</sub> cells, the percentage of PD-1<sup>hi</sup> SARS-CoV-2-specific memory cT<sub>FH</sub> dropped over time (Fig. 4J). CCR6<sup>+</sup> SARS-CoV-2-specific cT<sub>FH</sub> cells have been associated with reduced COVID-19 disease severity (5) and have been reported to be a major fraction of spike-specific cT<sub>FH</sub> cells in some studies (5, 50, 58). Here we confirmed that a significant fraction of both spike-specific and MP\_R memory cT<sub>FH</sub> cells were CCR6<sup>+</sup>. We also observed increases in CCR6<sup>+</sup> cT<sub>FH</sub> memory over time ( $p = 0.001$  and  $p = 0.014$  at  $\geq 6$  months PSO compared to bulk cT<sub>FH</sub>, Fig. 4K). Overall, substantial cT<sub>FH</sub> memory was observed after SARS-CoV-2 infection, with a durability  $\geq 6$  months PSO.

### Immune memory relationships

Immune memory to SARS-CoV-2 was considered, including relationships between the compartments of immune memory. Males had higher spike IgG [analysis of covariance (ANCOVA)  $p = 0.00018$ , Fig. 5A] and RBD and nucleocapsid IgG (ANCOVA  $p = 0.00077$  and  $p = 0.018$ ; fig. S6, A and B), consistent with other studies (46, 47). Higher spike IgG was also observed in males when only nonhospitalized cases were considered (ANCOVA  $p = 0.00025$ , fig. S6C). By contrast, no differences were observed in IgA or PSV neutralization titers (fig. S6, D to F), and no differences were detected in SARS-CoV-2 memory B cell, memory CD8<sup>+</sup> T cell, or memory CD4<sup>+</sup> T cell frequencies between males and females (fig. S6, G to K).

Immune memory was examined for associations between magnitude of memory and COVID-19 disease severity. The number of previously hospitalized COVID-19 cases ( $n = 13$ ) limited analysis options. However, the cases

were well distributed between males and females (Table 1), data from large numbers of nonhospitalized cases were available for comparison, and the analyses in Figs. 1 to 4 demonstrated that immune memory was relatively stable over the time window analyzed. Therefore, we could simplify the disease severity analysis by grouping all samples from 120+ days PSO [also limiting data to a single sample per subject (figs. S7 to S9); most of the previously hospitalized subjects were sampled at two time points, fig. S7A] and then comparing nonhospitalized and hospitalized subjects. Spike and RBD IgG titers in hospitalized cases were higher than in nonhospitalized cases (Fig. 5B), consistent with other studies (46, 47). Spike and RBD-specific memory B cell frequencies were also higher in hospitalized cases (~1.7-fold and ~2.5-fold, respectively; Fig. 5C and fig. S8). By contrast, memory CD8<sup>+</sup> T cell frequencies were not higher in hospitalized cases compared to nonhospitalized cases (Fig. 5D and fig. S9), and memory CD4<sup>+</sup> T cell frequencies trended lower in hospitalized cases compared to nonhospitalized cases (Fig. 5E and fig. S9). Therefore, although our conclusions are limited by the number of hospitalized subjects, increased spike IgG titers were consistent across three independent studies, and increased memory B cells among hospitalized cases were observed here (not measured in other studies), indicating that both compartments of long-term humoral immunity to SARS-CoV-2 are higher in individuals who experienced a more severe COVID-19 disease course. T cell memory did not follow the same pattern, consistent with indications that hospitalized cases of COVID-19 can be associated with poorer T cell responses in the acute phase (5, 59). Additionally, these data show that, although gender and COVID-19 disease severity contribute to differences in immune memory to SARS-CoV-2, neither factor could account for the majority of the heterogeneity in immune memory to this virus.

Very few published data sets compare antigen-specific antibody, B cell, CD8<sup>+</sup> T cell, and CD4<sup>+</sup> T cell memory to an acute viral infection in the same individuals. We therefore made use of this combined data set to examine interrelationships between compartments of immune memory. We focused on RBD IgG, RBD memory B cells, spike IgA, total SARS-CoV-2-specific CD8<sup>+</sup> T cells, and total SARS-CoV-2-specific CD4<sup>+</sup> T cells, owing to their putative potential roles in protective immunity. The majority (64%) of COVID-19 cases were positive for all five of these immune memory compartments at 1 to 2 months PSO (Fig. 5, F and G), with the incomplete responses largely reflecting individuals with no detectable CD8<sup>+</sup> T cell memory and/or poor IgA responses (Fig. 5G). At 5 to 8 months after COVID-19 infection, the proportion of individ-

uals positive for all five of these immune memory compartments had dropped to 43%; nevertheless, 95% of individuals were still positive for at least three out of five SARS-CoV-2 immune memory responses (Fig. 5G). Immune memory at 5 to 8 months PSO represented contributions from different immune memory compartments in different individuals (Fig. 5G). Similar results were obtained if RBD IgG was replaced by neutralizing antibodies (fig. S10A). Overall, these findings again highlight heterogeneity of immune memory, with different patterns of immune memory in different individuals.

Interrelationships between the components of memory were next examined by assessing ratios between immune memory compartments over time. The ratio of SARS-CoV-2 CD4<sup>+</sup> T cell memory to SARS-CoV-2 CD8<sup>+</sup> T cell memory was largely stable over time (Fig. 5H and fig. S10B). Given that serological measurements are the simplest measurements of immune memory at a population scale, we examined how well such serological measurements may serve as surrogate markers of other components of SARS-CoV-2 immune memory over time. The relationship between circulating RBD IgG and RBD-specific memory B cells changed ~20-fold over the time range studied ( $R = 0.60$ , Fig. 5H and fig. S10C). The changing relationship between circulating spike IgA and RBD-specific memory B cells was even larger ( $R = 0.55$ , Fig. 5H and fig. S10D). The relationship between RBD IgG and SARS-CoV-2 CD4<sup>+</sup> T cell memory was relatively flat over the time range studied (Fig. 5H); however, variation spanned a ~1000-fold range (fig. S10E). Thus, predictive power of circulating RBD IgG for assessing T cell memory was poor because of the heterogeneity between individuals ( $R = 0.046$ ). In sum, although heterogeneity of immune responses is a defining feature of COVID-19, immune memory to SARS-CoV-2 develops in almost all subjects, with complex relationships between the individual immune memory compartments.

### Concluding remarks

In this study, we aimed to fill gaps in our basic understanding of immune memory after COVID-19. This required simultaneous measurement of circulating antibodies, memory B cells, CD8<sup>+</sup> T cells, and CD4<sup>+</sup> T cells specific for SARS-CoV-2, in a group of subjects with a full range of disease, and distributed from short time points after infection to 8 months later. By studying these multiple compartments of adaptive immunity in an integrated manner, we observed that each component of SARS-CoV-2 immune memory exhibited distinct kinetics.

The spike IgG titers were durable, with modest declines in titers at 6 to 8 months PSO at the population level. RBD IgG and SARS-CoV-2 PSV-neutralizing antibody titers

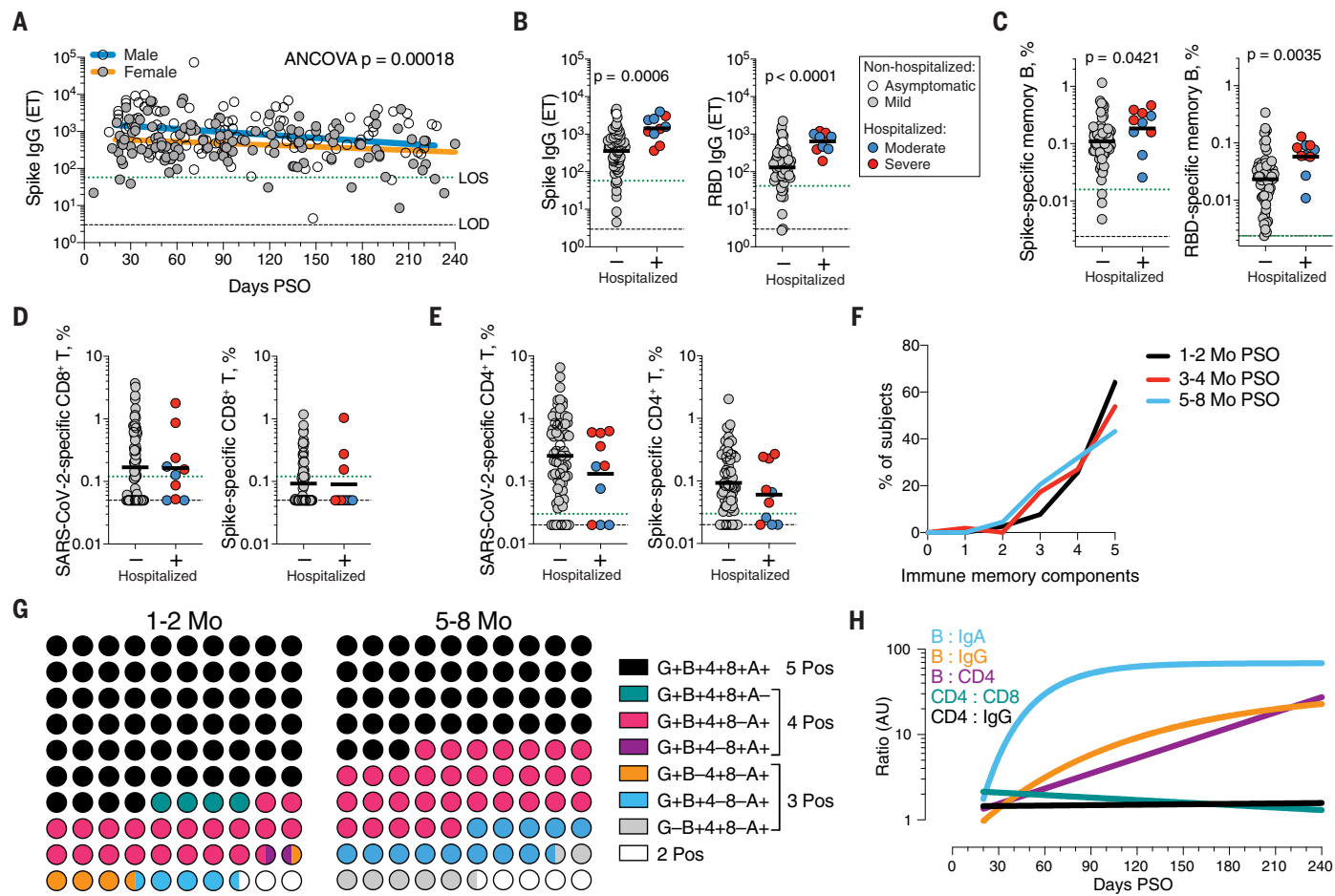


**Fig. 5. Immune memory relationships.** (A) Relationship between gender and spike IgG titers over time. Males: Linear decay preferred model,  $t_{1/2} = 110$  days; 95% CI: 65 to 349 days,  $R = -0.27$ ,  $p = 0.0046$ . Females: linear decay preferred model,  $t_{1/2} = 159$  days; 95% CI: 88 to 846 days,  $R = -0.22$ ,  $p = 0.016$ . ANCOVA  $p = 0.00018$ . Test for homogeneity of regressions  $F = 1.51$ ,  $p = 0.22$ . (B to E) Immune memory at 120+ days PSO in COVID-19 nonhospitalized and hospitalized subjects. Symbol colors represent peak disease severity (white: asymptomatic, gray: mild, blue: moderate, red: severe.) For subjects with multiple sample time points, only the final time point was used for these analyses. (B) Spike-specific IgG (left) and RBD-specific IgG (right) binding titers.  $n = 64$  (nonhospitalized),  $n = 10$  (hospitalized). Mann-Whitney U tests. (C) Frequency of memory B cells specific to spike (left) and RBD (right) at 120+ days PSO.  $n = 66$  (nonhospitalized),  $n = 10$  (hospitalized). Mann-Whitney U tests. (D) Frequency of total SARS-CoV-2-specific CD8<sup>+</sup> T cells (left) and spike-specific CD8<sup>+</sup> T cells (right).  $p = 0.72$  for total SARS-CoV-2-specific,  $p = 0.60$  for spike-specific by Mann-Whitney U tests.  $n = 72$  (nonhospitalized),  $n = 10$  (hospitalized). (E) Frequency of total SARS-CoV-2-specific CD4<sup>+</sup> T cells (left) and spike-specific CD4<sup>+</sup> T cells (right).  $p = 0.23$  for total SARS-CoV-2-specific,  $p = 0.24$  for spike-specific by Mann-Whitney U tests. (F) Immune

memory to SARS-CoV-2 during the early phase (1 to 2 mo, black line), medium phase (3 to 4 mo, red line), or late phase (5 to 8 mo, blue line). For each individual, a score of 1 was assigned for each response above LOS for RBD IgG, spike IgA, RBD-specific memory B cells, SARS-CoV-2-specific CD4<sup>+</sup> T cells, and SARS-CoV-2-specific CD8<sup>+</sup> T cells, giving a maximum total of five components of SARS-CoV-2 immune memory. Only COVID-19 convalescent subjects with all five immunological parameters tested were included in the analysis.  $n = 78$  (1 to 2 mo),  $n = 52$  (3 to 4 mo),  $n = 44$  (5 to 8 mo). (G) Percentage dot plots showing frequencies (normalized to 100%) of subjects with indicated immune memory components as described in (B) during the early (1 to 2 mo) or late (5 to 8 mo) phase. G, RBD-specific IgG; B, RBD-specific memory B cells; 4, SARS-CoV-2-specific CD4<sup>+</sup> T cells; 8, SARS-CoV-2-specific CD8<sup>+</sup> T cells; A, spike-specific IgA.  $n = 78$  (1 to 2 mo),  $n = 44$  (5 to 8 mo). (H) Relationships between immune memory compartments in COVID-19 subjects over time, as ratios (full curves and data shown in fig. S10, B to F). AU, arbitrary units, scaled from fig. S10, B to F; B:IgA, RBD-specific memory B cell ratio to spike IgA antibodies; B:IgG, RBD-specific memory B cell ratio to RBD IgG antibodies; B:CD4, RBD-specific memory B cell ratio to SARS-CoV-2-specific CD4<sup>+</sup> T cells; CD4:CD8, SARS-CoV-2-specific CD4<sup>+</sup> T cells ratio to SARS-CoV-2-specific CD8<sup>+</sup> T cells; CD4: IgG, SARS-CoV-2-specific CD4<sup>+</sup> T cells ratio to RBD IgG antibodies.

were potentially similarly stable, consistent with the RBD domain of spike being the dominant neutralizing antibody target. We collected data at two time points for most longitudinal individuals herein. It is well recognized that the magnitude of the antibody response against SARS-CoV-2 is highly heterogeneous between individuals. We ob-

served that heterogeneous initial antibody responses did not collapse into a homogeneous circulating antibody memory; rather, heterogeneity is also a central feature of immune memory to this virus. For antibodies, the responses spanned a ~200-fold range. Additionally, this heterogeneity means that long-term longitudinal studies will be required to

precisely define antibody kinetics to SARS-CoV-2. We are reporting the simplest statistical models that explain the data. These curve fits do not disprove more complex kinetics such as overlapping kinetics, but those models would require much denser longitudinal sampling in future studies. Biologically, IgG antibodies having a half-life of ~21 days, and the

magnitude of the antibody response over time, reflect antibodies produced first by short-lived plasma cells and then long-lived plasma cells, with affinity maturation also affecting the apparent magnitude in conventional binding assays and neutralization assays. Overall, at 5 to 8 months PSO, almost all individuals were positive for SARS-CoV-2 spike and RBD IgG.

Notably, memory B cells specific for the spike protein or RBD were detected in almost all COVID-19 cases, with no apparent half-life at 5 to 8 months after infection. Other studies of RBD memory B cells report similar findings (50, 60). B cell memory to some other infections has been observed to be long-lived, including 60+ years after smallpox vaccination (61), or 90+ years after infection with influenza (62). The memory T cell half-lives observed over 6+ months PSO in this cohort (~125 to 225 days for CD8<sup>+</sup> and ~94 to 153 days for CD4<sup>+</sup> T cells) were comparable to the 123 days  $t_{1/2}$  observed for memory CD8<sup>+</sup> T cells after yellow fever immunization (56). SARS-CoV-2 T cell memory at 6 months has also now been reported in another study (63). Notably, the durability of a fraction of the yellow fever virus-specific memory CD8<sup>+</sup> T cells possessed an estimated  $t_{1/2}$  of 485 days by deuterium labeling (56). Using different approaches, studies determined the long-term durability of memory CD4<sup>+</sup> T cells to smallpox, over a period of many years, to be an estimated  $t_{1/2}$  of ~10 years (61, 64), which is also consistent with recent detection of SARS-CoV-specific T cells 17 years after the initial infection (65). These data suggest that T cell memory might reach a more stable plateau, or slower decay phase, beyond the first 8 months after infection.

Although immune memory is the source of long-term protective immunity, direct conclusions about protective immunity cannot be made on the basis of quantifying SARS-CoV-2 circulating antibodies, memory B cells, CD8<sup>+</sup> T cells, and CD4<sup>+</sup> T cells, because mechanisms of protective immunity against SARS-CoV-2 or COVID-19 are not defined in humans. Nevertheless, some reasonable interpretations can be made. Antibodies are the only component of immune memory that can provide truly sterilizing immunity. Immunization studies in nonhuman primates have indicated that circulating neutralization titers of ~200 may provide sterilizing immunity against a relatively high-dose URT challenge (66), and neutralizing titers of ~3400 may provide sterilizing immunity against a very high dose URT challenge (67), although direct comparisons are not possible because the neutralizing antibody assays have not been standardized (3). Conclusions are also constrained by the limited overall amount of data on protective immunity to SARS-CoV-2.

Beyond sterilizing immunity, immune responses that confine SARS-CoV-2 to the URT

and oral cavity would minimize COVID-19 disease severity to that of a “common cold” or asymptomatic disease. This outcome is the primary goal of current COVID-19 vaccine clinical trials (3, 68). Such an outcome could potentially be mediated by a mixture of memory CD4<sup>+</sup> T cells, memory CD8<sup>+</sup> T cells, and memory B cells specific for RBD-producing anamnestic neutralizing antibodies, based on mechanisms of action in mouse models of other viral infections (69–71). In human COVID-19 infections, SARS-CoV-2-specific CD4<sup>+</sup> T cells and CD8<sup>+</sup> T cells are associated with less COVID-19 disease severity during an ongoing SARS-CoV-2 infection (5). Rapid seroconversion was associated with substantially reduced viral loads in acute disease over 14 days (29). Both of those associations are consistent with the hypothesis that SARS-CoV-2 memory T cells and B cells would be capable of substantially limiting SARS-CoV-2 dissemination and/or cumulative viral load, resulting in reduced COVID-19 disease severity. The likelihood of such outcomes is also closely tied to the kinetics of the infection, as memory B and T cell responses can take 3 to 5 days to successfully respond to an infection. As noted above, given the relatively slow course of severe COVID-19 in humans, resting immune memory compartments can potentially contribute in meaningful ways to protective immunity against pneumonia or severe secondary COVID-19. The presence of substerilizing neutralizing antibody titers at the time of SARS-CoV-2 exposure would blunt the size of the initial infection, and may provide an added contribution to limiting COVID-19 severity, on the basis of observations of protective immunity for other human respiratory viral infections (37, 72–74) and observations of SARS-CoV-2 vaccines in nonhuman primates (48, 67, 75).

The current study has some limitations. Longitudinal data for each subject, with at least three time points per subject, would be required for more precise understanding of the kinetics of durability of SARS-CoV-2-specific antibodies. Nevertheless, the current cross-sectional data describe well the dynamics of SARS-CoV-2 memory B cells, CD8<sup>+</sup> T cell, and CD4<sup>+</sup> T cell over 8 months PSO. This study was not sufficiently powered to control for many variables simultaneously. Additionally, circulating memory was assessed here; it is possible that local URT immune memory is a minimal, moderate, or large component of immune memory after a primary infection with SARS-CoV-2. This remains to be determined.

Individual case reports show that reinfections with SARS-CoV-2 are occurring (76, 77). However, a 2800-person study found no symptomatic re-infections over a ~118-day window (78), and a 1246-person study observed no symptomatic reinfections over 6 months (79).

We observed heterogeneity in the magnitude of adaptive immune responses to SARS-CoV-2 persisting into the immune memory phase. It is therefore possible that a fraction of the SARS-CoV-2-infected population with low immune memory would become susceptible to reinfection relatively soon. Although gender and disease severity both contribute to the heterogeneity of immune memory reported here, the source of much of the heterogeneity in immune memory to SARS-CoV-2 is unknown and worth further examination. Perhaps heterogeneity derives from low cumulative viral load or a small initial inoculum in some individuals. Nevertheless, our data show immune memory in at least three immunological compartments was measurable in ~95% of subjects 5 to 8 months PSO, indicating that durable immunity against secondary COVID-19 disease is a possibility in most individuals.

## Materials and methods

### Human subjects

The Institutional Review Boards of the University of California, San Diego (UCSD; 200236X) and the La Jolla Institute for Immunology (LJI; VD-214) approved the protocols used for blood collection for subjects with COVID-19 who donated at all sites other than Mount Sinai. The Icahn School of Medicine at Mount Sinai IRB approved the samples collected at this institution in New York City (IRB-16-00791). All human subjects were assessed for medical decision-making capacity using a standardized, approved assessment and voluntarily gave informed consent before being enrolled in the study. Study inclusion criteria included a diagnosis of COVID-19 or suspected COVID-19, age of 18 years or greater, and willingness and ability to provide informed consent. Although not a strict inclusion criterion, evidence of positive polymerase chain reaction (PCR)-based testing for SARS-CoV-2 was requested from subjects before participation. A total of 145 cases were confirmed SARS-CoV-2 positive by PCR-based testing (Table 1). Two subjects tested negative by SARS-CoV-2 PCR (Table 1). The remainder were not tested or did not have test results available for review (Table 1). Subjects who had a medical history and/or symptoms consistent with COVID-19, but lacked positive PCR-based testing for SARS-CoV-2 and subsequently had negative laboratory-based serologic testing for SARS-CoV-2, were then excluded; i.e., all COVID-19 cases in this study were confirmed cases by SARS-CoV-2 PCR or SARS-CoV-2 serodiagnostics, or both. Adults of all races, ethnicities, ages, and genders were eligible to participate. Study exclusion criteria included lack of willingness to participate, lack of ability to provide informed consent, or a medical contraindication to blood donation (e.g., severe anemia). Subject samples at LJI were obtained from

individuals in California and at least seven other states.

Blood collection and processing methods at LJI were performed as previously described (5). Briefly, whole blood was collected via phlebotomy in acid citrate dextrose (ACD) serum separator tubes (SST) or ethylenediaminetetraacetic acid (EDTA) tubes and processed for peripheral blood mononuclear cells (PBMCs), serum, and plasma isolation. Most donors were screened for symptoms prior to scheduling blood draws and had to be symptom-free and approximately 3 to 4 weeks out from symptom onset at the time of the initial blood draw at UCSD or LJI, respectively. Samples were coded, and then deidentified before analysis. Other efforts to maintain the confidentiality of participants included the labeling samples with coded identification numbers. An overview of the characteristics of subjects with COVID-19 is provided in Table 1.

COVID-19 disease severity was scored from 0 to 10 using a numerical scoring system based on the NIH ordinal scale (5, 80). A categorical descriptor was applied based on this scoring system: “asymptomatic” for a score of 1, “mild” for a score of 2 to 3, “moderate” for a score of 4 to 5, and “severe” for a score of 6 or more. Subjects with a numerical score of 4 or higher required hospitalization (including admission for observation) for management of COVID-19. Only one of 13 hospitalized subjects is shared from the previous study of acute COVID-19 (5). The days PSO was determined based on the difference between the date of the blood collection and the date of first reported symptoms consistent with COVID-19. For asymptomatic subjects, the day from first positive SARS-CoV-2 PCR-based testing was used in place of the date of first reported COVID-19 symptoms.

#### Recombinant proteins

Stabilized spike protein [2P (81)] and the RBD were expressed in HEK293F cells. Briefly, DNA expressing stabilized spike protein and RBD were subcloned into separate phCMV vectors and transfected into HEK293F cells at a ratio of 1 mg of DNA to 1 liter of cells. The cells were cultured at 37°C in a shaker incubator set to 125 rpm, 80% humidity, and 8% CO<sub>2</sub>. When cell viability dropped below 80% (typically 4 to 5 days), media was harvested and centrifuged to remove cells. Biolock reagent was added to the supernatant media to remove any excess biotin. The media was then filtered through a 0.22-μm filter to remove Biolocked aggregates. Proteins were purified using Streptrap HP 5 ml columns (Cytiva) using 100 mM Tris, 100 mM NaCl as the wash buffer and 100 mM Tris, 100 mM NaCl, 2.5 mM d-Desthiobiotin as the elution buffer. The eluted fractions for spike proteins were concentrated on 100-kDa Amicon filters and the RBDs were

concentrated on 10-kDa filters. The samples were further purified using S6increase columns for the spike variants and S200increase column for the RBD.

#### SARS-CoV-2 ELISAs

SARS-CoV-2 ELISAs were performed as previously described (2, 5, 82). Briefly, Corning 96-well half-area plates (ThermoFisher 3690) were coated with 1 μg/ml of antigen overnight at 4°C. Antigens included recombinant SARS-CoV-2 RBD protein, recombinant spike protein, and recombinant nucleocapsid protein (GenScript Z03488) [recombinant nucleocapsid antigens were also tested from Sino Biological (40588-V07E) and Invivogen (his-sars2-n) and yielded comparable results to GenScript nucleocapsid]. The following day, plates were blocked with 3% milk in phosphate-buffered saline (PBS) containing 0.05% Tween-20 for 1.5 hours at room temperature. Plasma was heat inactivated at 56°C for 30 to 60 min. Plasma was diluted in 1% milk containing 0.05% Tween-20 in PBS starting at a 1:3 dilution followed by serial dilutions by three and incubated for 1.5 hours at room temperature. Plates were washed five times with 0.05% PBS-Tween-20. Secondary antibodies were diluted in 1% milk containing 0.05% Tween-20 in PBS. For IgG, anti-human IgG peroxidase antibody produced in goat (Sigma A6029) was used at a 1:5,000 dilution. For IgA, anti-human IgA horseradish peroxidase antibody (Hybridoma Reagent Laboratory HP6123-HRP) was used at a 1:1,000 dilution. The HP6123 monoclonal anti-IgA was used because of its CDC- and WHO-validated specificity for human IgA1 and IgA2 and lack of cross-reactivity with non-IgA isotypes (83).

End-point titers were plotted for each sample, using background-subtracted data. Negative and positive controls were used to standardize each assay and normalize across experiments. A positive control standard was created by pooling plasma from six convalescent COVID-19 donors to normalize between experiments. The limit of detection (LOD) was defined as 1:3 for IgG, 1:10 for IgA. Limit of sensitivity (LOS) for SARS-CoV-2-infected individuals was established on the basis of uninfected subjects, using plasma from normal healthy donors never exposed to SARS-CoV-2. For cross-sectional analyses, modeling for the best fit curve (e.g., one phase decay versus simple linear regression) was performed using GraphPad Prism 8.0. Best curve fit was defined by an extra sum-of-squares F Test, selecting the simpler model unless  $P < 0.05$  (84). Continuous decay (linear regression), one-phased decay, or two-phased decay of log data were assessed in all cases, with the best fitting statistical model chosen on the basis of the F test; in several cases, a quadratic equation fit was also considered. To calculate the  $t_{1/2}$ , log<sub>2</sub>-transformed data were utilized. Using the

best fit curve, either a one-phase decay nonlinear fit or a simple linear regression (continuous decay) was utilized. For simple linear regressions, Pearson’s  $R$  was calculated for correlation using log<sub>2</sub>-transformed data. For one-phase decay nonlinear fit,  $R$  was reported. For longitudinal samples, a simple linear regression was performed, with  $t_{1/2}$  calculated from log<sub>2</sub>-transformed data for each pair. For gender analyses, modeling and  $t_{1/2}$  were performed similar to cross-sectional analyses; ANCOVA (VassarStats or GraphPad Prism 8.4) was then performed between male and female data sets. ANCOVA  $p$ -values of the adjusted means were reported and considered significant if the test for homogeneity of regressions was not significant.

#### Neutralizing antibody assays

The pseudovirus-neutralizing antibody assay was performed as previously described (5). Briefly, Vero cells were seeded in 96-well plates to produce a monolayer at the time of infection. Pretitrated amounts of rVSV-SARS-CoV-2 [phCMV3-SARS-CoV-2 spike SARS-CoV-2-psuedotype VSV-ΔG-GFP (green fluorescent protein)] were generated by transfecting HEK293T cells, ATCC CRL-3216] were incubated with serially diluted human plasma at 37°C for 1 hour before addition to confluent Vero cell monolayers (ATCC CCL-81) in 96-well plates. Cells were incubated for 12 to 16 hours at 37°C in 5% CO<sub>2</sub>. Cells were then fixed in 4% paraformaldehyde, stained with 1 μg/ml Hoechst, and imaged using a CellInsight CX5 imager to quantify the total number of cells expressing GFP. Infection was normalized to the average number of cells infected with rVSV-SARS-CoV-2 incubated with normal human plasma. The LOD was established as <1:20 on the basis of plasma samples from a series of unexposed control subjects. Negative signals were set to 1:19. Neutralization IC<sub>50</sub> (median inhibitory concentration) titers were calculated using One-Site Fit LogIC50 regression in GraphPad Prism 8.0.

#### Detection of antigen-specific memory B cells

To detect SARS-CoV-2 specific B cells, biotinylated protein antigens were individually multimerized with fluorescently labeled streptavidin at 4°C for 1 hour. Full-length SARS-CoV-2 spike (2P-stabilized, double Strep-tagged) and RBD were generated in-house. Biotinylation was performed using biotin-protein ligase standard reaction kit (Avidity, catalog no. Bir500A) following the manufacturer’s standard protocol and dialyzed overnight against PBS. Biotinylated spike was mixed with streptavidin BV421 (BioLegend, catalog no. 405225) and streptavidin Alexa Fluor 647 (Thermo Fisher Scientific, catalog no. S21374) at 20:1 ratio (~6:1 molar ratio). Biotinylated RBD was

mixed with streptavidin phycoerythrin (PE)/Cyanine7 (BioLegend, catalog no. 405206) at 2.2:1 ratio (~4:1 molar ratio). Biotinylated SARS-CoV-2 full-length nucleocapsid (Avi- and His-tagged; Sino Biological, catalog no. 40588-V27B-B) was multimerized using streptavidin PE (BioLegend, catalog no. 405204) and streptavidin BV711 (BioLegend, catalog no. 405241) at 5.5:1 ratio (~6:1 molar ratio). Streptavidin PE/Cyanine5.5 (Thermo Fisher Scientific, catalog no. SA1018) was used as a decoy probe to gate out SARS-CoV-2 non-specific streptavidin-binding B cells. The antigen probes prepared individually as above were then mixed in Brilliant Buffer (BD Bioscience, catalog no. 566349) containing 5  $\mu$ M free d-biotin (Avidity, catalog no. Bir500A). Free d-biotin ensured minimal cross-reactivity of antigen probes. About  $10^7$  previously frozen PBMC samples were prepared in U-bottom 96-well plates and stained with 50  $\mu$ l of antigen probe cocktail containing 100 ng of spike per probe (total 200ng), 27.5 ng of RBD, 40 ng of nucleocapsid per probe (total 80 ng), and 20 ng of streptavidin PE/Cyanine5.5 at 4°C for 1 hour to ensure maximal staining quality before surface staining with antibodies as listed in table S1 was performed in Brilliant Buffer at 4°C for 30 min. Dead cells were stained using LIVE/DEAD Fixable Blue Stain Kit (Thermo Fisher Scientific, catalog no. L34962) in DPBS at 4°C for 30 min. About 80% of antigen-specific memory (IgD<sup>+</sup> and/or CD27<sup>+</sup>) B cells detected using this method were IgM<sup>+</sup>, IgG<sup>+</sup>, or IgM<sup>-</sup> IgG<sup>-</sup> IgA<sup>+</sup>, which were comparable to nonspecific memory B cells. On the basis of these observations, we concluded that the antigen probes did not substantially affect the quality of surface immunoglobulin staining. Stained PBMC samples were acquired on Cytek Aurora and analyzed using FlowJo10.7.1 (BD Bioscience).

The frequency of antigen-specific memory B cells was expressed as a percentage of total B cells (CD19<sup>+</sup> CD20<sup>+</sup> CD38<sup>int/-</sup>, CD3<sup>+</sup>, CD14<sup>+</sup>, CD16<sup>+</sup>, CD56<sup>+</sup>, LIVE/DEAD<sup>+</sup>, lymphocytes), or as number per  $10^6$  PBMCs (LIVE/DEAD<sup>-</sup> cells). LOD was set on the basis of median + 2  $\times$  standard deviation (SD) of [1/(number of total B cells recorded)] or median + 2  $\times$  SD of [ $10^6$  / (number of PBMCs recorded)]. LOS was set as the median + 2  $\times$  SD of the results in unexposed donors. Phenotype analysis of antigen-specific B cells was performed only in subjects with at least 10 cells detected in the respective antigen-specific memory B cell gate. In each experiment, PBMCs from a known positive control (COVID-19 convalescent subject) and unexposed subjects were included to ensure consistent sensitivity and specificity of the assay. For each data set, second-order polynomial, simple linear regression, and pseudo-first-order kinetic models were considered. The model with a lower Akaike's information

criterion value was determined to be a better fit and visualized.

#### Activation-induced markers (AIM) T cell assay

Antigen-specific CD4<sup>+</sup> T cells were measured as a percentage of AIM<sup>+</sup> (OX40<sup>+</sup>CD137<sup>+</sup>) CD4<sup>+</sup> T and (CD69<sup>+</sup>CD137<sup>+</sup>) CD8<sup>+</sup> T cells after stimulation of PBMCs with overlapping peptide megapools (MPs) spanning the entire SARS-CoV-2 ORFeome, as previously described (2). Cells were cultured for 24 hours in the presence of SARS-CoV-2-specific MPs (1  $\mu$ g/ml) or 5  $\mu$ g/ml phytohemagglutinin (PHA, Roche) in 96-wells U-bottom plates at  $1 \times 10^6$  PBMCs per well. Stimulation with an equimolar amount of dimethyl sulfoxide (DMSO) was performed as a negative control. PHA and stimulation with a combined CD4<sup>+</sup> and CD8<sup>+</sup> cytomegalovirus epitope MP (CMV, 1  $\mu$ g/ml) were included as positive controls. Any sample with a low PHA signal was excluded as a quality control.

Antigen-specific CD4<sup>+</sup> and CD8<sup>+</sup> T cells were measured as background (DMSO)-subtracted data, with a minimal DMSO level set to 0.005%. All positive ORFs (>0.02% for CD4<sup>+</sup>, >0.05% for CD8<sup>+</sup>) were then aggregated into a combined sum of SARS-CoV-2-specific CD4<sup>+</sup> or CD8<sup>+</sup> T cells. The threshold for positivity for antigen-specific CD4<sup>+</sup> T cell responses (0.03%) and antigen-specific CD8<sup>+</sup> T cell responses (0.12%) was calculated using the median twofold standard deviation of all negative controls measured (>150). The antibody panel utilized in the (OX40<sup>+</sup>CD137<sup>+</sup>) CD4<sup>+</sup> T and (CD69<sup>+</sup>CD137<sup>+</sup>) CD8<sup>+</sup> T cells AIM staining is shown in table S2. A consistency analysis was performed for multiple measurements of AIM T cell assays by two different operators. Before merging, we compared the protein immunodominance, total SARS-CoV-2-specific CD4<sup>+</sup> and CD8<sup>+</sup> T cell responses, and half-life calculations between the two groups of experimental data. In longitudinal analyses, half-life calculations excluded any samples that were negative at both time points (because a half-life could not be calculated), though all data were included in the graphs.

For surface CD40L<sup>+</sup> OX40<sup>+</sup> CD4<sup>+</sup> T cell AIM assays, experiments were performed as previously described (5), with the following modifications. Cells were cultured in complete RPMI containing 5% human AB serum (Gemini Bioproducts),  $\beta$ -mercaptoethanol, penicillin/streptomycin, sodium pyruvate (NaPy), and nonessential amino acids. Prior to addition of peptide MPs, cells were blocked at 37°C for 15 min with 0.5  $\mu$ g/ml of anti-CD40 mAb (Miltenyi Biotec). A stimulation with an equimolar amount of DMSO was performed to determine background subtraction, and activation from staphylococcal enterotoxin B (SEB) at 1  $\mu$ g/ml was used as a (positive) quality control. LOD for antigen-specific cT<sub>FH</sub> among CD4<sup>+</sup> T cells was based on the LOD for

antigen-specific CD4<sup>+</sup> T cells (described above) multiplied by the average % cT<sub>FH</sub> in the bulk CD4 T cells among control samples. An inclusion threshold of ten events after the cT<sub>FH</sub> CXCR5<sup>+</sup> gate was used for PD-1<sup>hi</sup> and CCR6<sup>+</sup> calculations, and Mann-Whitney nonparametric and Wilcoxon signed-rank statistical tests were applied for the respective comparisons.

#### REFERENCES AND NOTES

- D. S. Stephens, M. J. McElrath, COVID-19 and the Path to Immunity. *JAMA* **324**, 1279–1281 (2020). doi: [10.1001/jama.2020.16656](https://doi.org/10.1001/jama.2020.16656); pmid: [32915201](https://pubmed.ncbi.nlm.nih.gov/32915201/)
- A. Grifoni et al., Targets of T Cell Responses to SARS-CoV-2 Coronavirus in Humans with COVID-19 Disease and Unexposed Individuals. *Cell* **181**, 1489–1501.e15 (2020). doi: [10.1016/j.cell.2020.05.015](https://doi.org/10.1016/j.cell.2020.05.015); pmid: [32473127](https://pubmed.ncbi.nlm.nih.gov/32473127/)
- F. Krammer, SARS-CoV-2 vaccines in development. *Nature* **586**, 516–527 (2020). doi: [10.1038/s41586-020-2798-3](https://doi.org/10.1038/s41586-020-2798-3); pmid: [32967006](https://pubmed.ncbi.nlm.nih.gov/32967006/)
- M. S. Suthar et al., Rapid generation of neutralizing antibody responses in COVID-19 patients. *Cell Rep. Med.* **1**, 100040 (2020). doi: [10.1016/j.xcrm.2020.100040](https://doi.org/10.1016/j.xcrm.2020.100040); pmid: [32835303](https://pubmed.ncbi.nlm.nih.gov/32835303/)
- C. Rydzynski Maderbacher et al., Antigen-specific adaptive immunity to SARS-CoV-2 in acute COVID-19 and associations with age and disease severity. *Cell* **183**, 996–1012.e19 (2020). doi: [10.1016/j.cell.2020.09.038](https://doi.org/10.1016/j.cell.2020.09.038); pmid: [33010815](https://pubmed.ncbi.nlm.nih.gov/33010815/)
- R. Zhou et al., Acute SARS-CoV-2 infection impairs dendritic cell and T cell responses. *Immunity* **53**, 864–877.e5 (2020). doi: [10.1016/j.jimmuni.2020.07.026](https://doi.org/10.1016/j.jimmuni.2020.07.026); pmid: [32791036](https://pubmed.ncbi.nlm.nih.gov/32791036/)
- M. Liao et al., Single-cell landscape of bronchoalveolar immune cells in patients with COVID-19. *Nat. Med.* **26**, 842–844 (2020). doi: [10.1038/s41591-020-0901-9](https://doi.org/10.1038/s41591-020-0901-9); pmid: [32398875](https://pubmed.ncbi.nlm.nih.gov/32398875/)
- A. G. Laing et al., A dynamic COVID-19 immune signature includes associations with poor prognosis. *Nat. Med.* **26**, 1623–1635 (2020). doi: [10.1038/s41591-020-1038-6](https://doi.org/10.1038/s41591-020-1038-6); pmid: [32807934](https://pubmed.ncbi.nlm.nih.gov/32807934/)
- D. Blanco-Melo et al., Imbalanced Host Response to SARS-CoV-2 Drives Development of COVID-19. *Cell* **181**, 1036–1045.e9 (2020). doi: [10.1016/j.cell.2020.04.026](https://doi.org/10.1016/j.cell.2020.04.026); pmid: [32416070](https://pubmed.ncbi.nlm.nih.gov/32416070/)
- P. S. Arunachalam et al., Systems biological assessment of immunity to mild versus severe COVID-19 infection in humans. *Science* **369**, 1210–1220 (2020). doi: [10.1126/science.abc6261](https://doi.org/10.1126/science.abc6261); pmid: [32788292](https://pubmed.ncbi.nlm.nih.gov/32788292/)
- P. Bastard et al., Autoantibodies against type I IFNs in patients with life-threatening COVID-19. *Science* **370**, eabd4585 (2020). doi: [10.1126/science.abd4585](https://doi.org/10.1126/science.abd4585); pmid: [32972996](https://pubmed.ncbi.nlm.nih.gov/32972996/)
- Q. Zhang et al., Inborn errors of type I IFN immunity in patients with life-threatening COVID-19. *Science* **370**, eabd4570 (2020). doi: [10.1126/science.abd4570](https://doi.org/10.1126/science.abd4570); pmid: [32972995](https://pubmed.ncbi.nlm.nih.gov/32972995/)
- D. M. Del Valle et al., An inflammatory cytokine signature predicts COVID-19 severity and survival. *Nat. Med.* **26**, 1636–1643 (2020). doi: [10.1038/s41591-020-1051-9](https://doi.org/10.1038/s41591-020-1051-9); pmid: [32839624](https://pubmed.ncbi.nlm.nih.gov/32839624/)
- L. Kuri-Cervantes et al., Comprehensive mapping of immune perturbations associated with severe COVID-19. *Sci. Immunol.* **5**, eabd7114 (2020). doi: [10.1126/sciimmunol.abd7114](https://doi.org/10.1126/sciimmunol.abd7114); pmid: [32669287](https://pubmed.ncbi.nlm.nih.gov/32669287/)
- S. Li et al., Clinical and pathological investigation of patients with severe COVID-19. *JCI Insight* **5**, (2020). doi: [10.1172/jci.insight.138070](https://doi.org/10.1172/jci.insight.138070); pmid: [32427582](https://pubmed.ncbi.nlm.nih.gov/32427582/)
- C. Radermecker et al., Neutrophil extracellular traps infiltrate the lung airway, interstitial, and vascular compartments in severe COVID-19. *J. Exp. Med.* **217**, e20201012 (2020). doi: [10.1084/jem.20201012](https://doi.org/10.1084/jem.20201012); pmid: [32926097](https://pubmed.ncbi.nlm.nih.gov/32926097/)
- B. Schurink et al., Viral presence and immunopathology in patients with lethal COVID-19: A prospective autopsy cohort study. *Lancet Microbe* **1**, e290–e299 (2020). doi: [10.1016/S2666-5247\(20\)30144-0](https://doi.org/10.1016/S2666-5247(20)30144-0); pmid: [33015653](https://pubmed.ncbi.nlm.nih.gov/33015653/)
- M. Aid et al., Vascular Disease and Thrombosis in SARS-CoV-2-Infected Rhesus Macaques. *Cell* **183**, 1354–1366.e13 (2020). doi: [10.1016/j.cell.2020.10.005](https://doi.org/10.1016/j.cell.2020.10.005); pmid: [33065030](https://pubmed.ncbi.nlm.nih.gov/33065030/)
- N. Baumgarth, J. Nikolicz-Zugich, F. E.-H. Lee, D. Bhattacharya, Antibody Responses to SARS-CoV-2: Let's Stick to Known Knowns. *J. Immunol.* **205**, 2342–2350 (2020). doi: [10.4049/jimmunol.2000839](https://doi.org/10.4049/jimmunol.2000839); pmid: [32887754](https://pubmed.ncbi.nlm.nih.gov/32887754/)
- A. Wajnberg et al., Robust neutralizing antibodies to SARS-CoV-2 infection persist for months. *Science* **370**, 1227–1230 (2020). doi: [10.1126/science.abd7728](https://doi.org/10.1126/science.abd7728); pmid: [33115920](https://pubmed.ncbi.nlm.nih.gov/33115920/)

21. A. Sariol, S. Perlman, Lessons for COVID-19 immunity from other coronavirus infections. *Immunity* **53**, 248–263 (2020). doi: [10.1016/j.jimmuni.2020.07.005](https://doi.org/10.1016/j.jimmuni.2020.07.005); pmid: [32717182](https://pubmed.ncbi.nlm.nih.gov/32717182/)
22. K. Subbarao, SARS-CoV-2: A New Song Recalls an Old Melody. *Cell Host Microbe* **27**, 692–694 (2020). doi: [10.1016/j.chom.2020.04.019](https://doi.org/10.1016/j.chom.2020.04.019); pmid: [32407706](https://pubmed.ncbi.nlm.nih.gov/32407706/)
23. W. Deng et al., Primary exposure to SARS-CoV-2 protects against reinfection in rhesus macaques. *Science* **369**, 818–823 (2020). doi: [10.1126/science.abc5343](https://doi.org/10.1126/science.abc5343); pmid: [32616673](https://pubmed.ncbi.nlm.nih.gov/32616673/)
24. Q. Gao et al., Development of an inactivated vaccine candidate for SARS-CoV-2. *Science* **369**, 77–81 (2020). doi: [10.1126/science.abc1932](https://doi.org/10.1126/science.abc1932); pmid: [32376603](https://pubmed.ncbi.nlm.nih.gov/32376603/)
25. A. Chandrasekhar et al., SARS-CoV-2 infection protects against rechallenge in rhesus macaques. *Science* **369**, 812–817 (2020). doi: [10.1126/science.abc4776](https://doi.org/10.1126/science.abc4776); pmid: [32434946](https://pubmed.ncbi.nlm.nih.gov/32434946/)
26. S. J. Zost et al., Potently neutralizing and protective human antibodies against SARS-CoV-2. *Nature* **584**, 443–449 (2020). doi: [10.1038/s41586-020-2548-6](https://doi.org/10.1038/s41586-020-2548-6); pmid: [32668443](https://pubmed.ncbi.nlm.nih.gov/32668443/)
27. T. F. Rogers et al., Isolation of potent SARS-CoV-2 neutralizing antibodies and protection from disease in a small animal model. *Science* **369**, 956–963 (2020). doi: [10.1126/science.abc7520](https://doi.org/10.1126/science.abc7520); pmid: [32540903](https://pubmed.ncbi.nlm.nih.gov/32540903/)
28. A. Baum et al., REGN-COV2 antibodies prevent and treat SARS-CoV-2 infection in rhesus macaques and hamsters. *Science* **370**, 1110–1115 (2020). doi: [10.1126/science.abe2402](https://doi.org/10.1126/science.abe2402); pmid: [33037066](https://pubmed.ncbi.nlm.nih.gov/33037066/)
29. D. M. Weinreich et al., REGN-COV2, a Neutralizing Antibody Cocktail, in Outpatients with Covid-19. *N. Engl. J. Med.* NEJMoa2035002 (2020). doi: [10.1056/NEJMoa2035002](https://doi.org/10.1056/NEJMoa2035002); pmid: [3332778](https://pubmed.ncbi.nlm.nih.gov/3332778/)
30. Lilly announces proof of concept data for neutralizing antibody LY-CoV555 in the COVID-19 outpatient setting | Eli Lilly and Company; <https://investor.lilly.com/news-releases/news-release-details/lilly-announces-proof-concept-data-neutralizing-antibodyid>
31. D. M. Altmann, R. J. Boyton, SARS-CoV-2 T cell immunity: Specificity, function, durability, and role in protection. *Sci. Immunol.* **5**, eabd6160 (2020). doi: [10.1126/sciimmunol.abd6160](https://doi.org/10.1126/sciimmunol.abd6160); pmid: [32680954](https://pubmed.ncbi.nlm.nih.gov/32680954/)
32. P. Van Damme, K. Van Herck, A review of the long-term protection after hepatitis A and B vaccination. *Travel Med. Infect. Dis.* **5**, 79–84 (2007). doi: [10.1016/j.tmaid.2006.04.004](https://doi.org/10.1016/j.tmaid.2006.04.004); pmid: [17298912](https://pubmed.ncbi.nlm.nih.gov/17298912/)
33. M. M. Rosado et al., Switched memory B cells maintain specific memory independently of serum antibodies: The hepatitis B example. *Eur. J. Immunol.* **41**, 1800–1808 (2011). doi: [10.1002/eji.201041187](https://doi.org/10.1002/eji.201041187); pmid: [21469123](https://pubmed.ncbi.nlm.nih.gov/21469123/)
34. F. Zhou et al., Clinical course and risk factors for mortality of adult inpatients with COVID-19 in Wuhan, China: A retrospective cohort study. *Lancet* **395**, 1054–1062 (2020). doi: [10.1016/S0140-6736\(20\)30566-3](https://doi.org/10.1016/S0140-6736(20)30566-3); pmid: [32171076](https://pubmed.ncbi.nlm.nih.gov/32171076/)
35. W. A. Orenstein, R. Ahmed, Simply put: Vaccination saves lives. *Proc. Natl. Acad. Sci. U.S.A.* **114**, 4031–4033 (2017). doi: [10.1073/pnas.1704507114](https://doi.org/10.1073/pnas.1704507114); pmid: [28396427](https://pubmed.ncbi.nlm.nih.gov/28396427/)
36. P. Piot et al., Immunization: Vital progress, unfinished agenda. *Nature* **575**, 119–129 (2019). doi: [10.1038/s41586-019-1656-7](https://doi.org/10.1038/s41586-019-1656-7); pmid: [31695203](https://pubmed.ncbi.nlm.nih.gov/31695203/)
37. S. Plotkin, W. Orenstein, P. Offit, *Plotkin's Vaccines* (Elsevier, ed. 7, 2018).
38. F. Sallusto, A. Lanzavecchia, K. Araki, R. Ahmed, From vaccines to memory and back. *Immunity* **33**, 451–463 (2010). doi: [10.1016/j.jimmuni.2010.10.008](https://doi.org/10.1016/j.jimmuni.2010.10.008); pmid: [21029957](https://pubmed.ncbi.nlm.nih.gov/21029957/)
39. S. Crotty, R. Ahmed, Immunological memory in humans. *Semin. Immunol.* **16**, 197–203 (2004). doi: [10.1016/j.smim.2004.02.008](https://doi.org/10.1016/j.smim.2004.02.008); pmid: [15130504](https://pubmed.ncbi.nlm.nih.gov/15130504/)
40. F. Weisel, M. Shlomchik, Memory B Cells of Mice and Humans. *Annu. Rev. Immunol.* **35**, 255–284 (2017). doi: [10.1146/annurev-immunol-041015-055531](https://doi.org/10.1146/annurev-immunol-041015-055531); pmid: [28142324](https://pubmed.ncbi.nlm.nih.gov/28142324/)
41. S. M. Kissler, C. Tedijanto, E. Goldstein, Y. H. Grad, M. Lipsitch, Projecting the transmission dynamics of SARS-CoV-2 through the postpandemic period. *Science* **368**, 860–868 (2020). doi: [10.1126/science.abb5793](https://doi.org/10.1126/science.abb5793); pmid: [32291278](https://pubmed.ncbi.nlm.nih.gov/32291278/)
42. C. M. Saad-Roy et al., Immune life history, vaccination, and the dynamics of SARS-CoV-2 over the next 5 years. *Science* **370**, 811–818 (2020). doi: [10.1126/science.abd7343](https://doi.org/10.1126/science.abd7343); pmid: [32958581](https://pubmed.ncbi.nlm.nih.gov/32958581/)
43. Q.-X. Long et al., Clinical and immunological assessment of asymptomatic SARS-CoV-2 infections. *Nat. Med.* **26**, 1200–1204 (2020). doi: [10.1038/s41591-020-0965-6](https://doi.org/10.1038/s41591-020-0965-6); pmid: [32555424](https://pubmed.ncbi.nlm.nih.gov/32555424/)
44. D. F. Gudbjartsson et al., Humoral Immune Response to SARS-CoV-2 in Iceland. *N. Engl. J. Med.* **383**, 1724–1734 (2020). doi: [10.1056/NEJMoa2026116](https://doi.org/10.1056/NEJMoa2026116); pmid: [32871063](https://pubmed.ncbi.nlm.nih.gov/32871063/)
45. A. Wajnberg et al., Robust neutralizing antibodies to SARS-CoV-2 infection persist for months. *Science* **370**, 1227–1230 (2020). doi: [10.1126/science.abd7728](https://doi.org/10.1126/science.abd7728); pmid: [33115920](https://pubmed.ncbi.nlm.nih.gov/33115920/)
46. L. Piccoli et al., Mapping neutralizing and immunodominant sites on the SARS-CoV-2 spike receptor-binding domain by structure-guided high-resolution serology. *Cell* **183**, 1024–1042.e21 (2020). doi: [10.1016/j.cell.2020.09.037](https://doi.org/10.1016/j.cell.2020.09.037); pmid: [32991844](https://pubmed.ncbi.nlm.nih.gov/32991844/)
47. D. F. Robbiani et al., Convergent antibody responses to SARS-CoV-2 in convalescent individuals. *Nature* **584**, 437–442 (2020). doi: [10.1038/s41586-020-2456-9](https://doi.org/10.1038/s41586-020-2456-9); pmid: [32555388](https://pubmed.ncbi.nlm.nih.gov/32555388/)
48. J. Yu et al., DNA vaccine protection against SARS-CoV-2 in rhesus macaques. *Science* **369**, 806–811 (2020). doi: [10.1126/science.abc6284](https://doi.org/10.1126/science.abc6284); pmid: [32434945](https://pubmed.ncbi.nlm.nih.gov/32434945/)
49. B. Isho et al., Persistence of serum and saliva antibody responses to SARS-CoV-2 spike antigens in COVID-19 patients. *Sci. Immunol.* **5**, eabe5511 (2020). doi: [10.1126/sciimmunol.abe5511](https://doi.org/10.1126/sciimmunol.abe5511); pmid: [33033173](https://pubmed.ncbi.nlm.nih.gov/33033173/)
50. L. B. Rodda et al., Functional SARS-CoV-2-specific immune memory persists after mild COVID-19. *Cell* **S0092-8674(20)31565-8** (2020). doi: [10.1016/j.cell.2020.11.029](https://doi.org/10.1016/j.cell.2020.11.029); pmid: [33296701](https://pubmed.ncbi.nlm.nih.gov/33296701/)
51. C. W. Davis et al., Longitudinal Analysis of the Human B Cell Response to Ebola Virus Infection. *Cell* **177**, 1566–1582.e17 (2019). doi: [10.1016/j.cell.2019.04.036](https://doi.org/10.1016/j.cell.2019.04.036); pmid: [31048480](https://pubmed.ncbi.nlm.nih.gov/31048480/)
52. A. Z. Wee et al., Longitudinal dynamics of the human B cell response to the yellow fever 17D vaccine. *Proc. Natl. Acad. Sci. U.S.A.* **117**, 6675–6685 (2020). doi: [10.1073/pnas.1921388117](https://doi.org/10.1073/pnas.1921388117); pmid: [32152119](https://pubmed.ncbi.nlm.nih.gov/32152119/)
53. M. F. Koturi et al., The CD8+ T-cell response to lymphocytic choriomeningitis virus involves the L antigen: Uncovering new tricks for an old virus. *J. Virol.* **81**, 4928–4940 (2007). doi: [10.1128/JVI.02632-06](https://doi.org/10.1128/JVI.02632-06); pmid: [17329346](https://pubmed.ncbi.nlm.nih.gov/17329346/)
54. J. Neidleman et al., SARS-CoV-2-specific T cells exhibit phenotypic features of helper function, lack of terminal differentiation, and high proliferation potential. *Cell Rep. Med.* **1**, 100081 (2020). doi: [10.1101/jxrm.2020.100081](https://doi.org/10.1101/jxrm.2020.100081); pmid: [32839763](https://pubmed.ncbi.nlm.nih.gov/32839763/)
55. S. Sridhar et al., Cellular immune correlates of protection against symptomatic pandemic influenza. *Nat. Med.* **19**, 1305–1312 (2013). doi: [10.1038/nm.3350](https://doi.org/10.1038/nm.3350); pmid: [24056771](https://pubmed.ncbi.nlm.nih.gov/24056771/)
56. R. S. Akondy et al., Origin and differentiation of human memory CD8 T cells after vaccination. *Nature* **552**, 362–367 (2017). doi: [10.1038/nature24633](https://doi.org/10.1038/nature24633); pmid: [29236685](https://pubmed.ncbi.nlm.nih.gov/29236685/)
57. S. Crotty, T Follicular Helper Cell Biology: A Decade of Discovery and Diseases. *Immunity* **50**, 1132–1148 (2019). doi: [10.1016/j.jimmuni.2019.04.011](https://doi.org/10.1016/j.jimmuni.2019.04.011); pmid: [3117010](https://pubmed.ncbi.nlm.nih.gov/3117010/)
58. J. A. Juno et al., Humoral and circulating follicular helper T cell responses in recovered patients with COVID-19. *Nat. Med.* **26**, 1428–1434 (2020). doi: [10.1038/s41591-020-0995-0](https://doi.org/10.1038/s41591-020-0995-0); pmid: [32661393](https://pubmed.ncbi.nlm.nih.gov/32661393/)
59. A. T. Tan et al., Early induction of SARS-CoV-2 specific T cells associates with rapid viral clearance and mild disease in COVID-19 patients. *bioRxiv* 2020.10.15.341958 [Preprint]. 16 October 2020. <https://doi.org/10.1101/2020.10.15.341958>
60. C. Gaebler et al., Evolution of Antibody Immunity to SARS-CoV-2. *bioRxiv* 2020.11.03.367391 (2020). doi: [10.1101/2020.11.03.367391](https://doi.org/10.1101/2020.11.03.367391); pmid: [33173867](https://pubmed.ncbi.nlm.nih.gov/33173867/)
61. S. Crotty et al., Cutting edge: Long-term B cell memory in humans after smallpox vaccination. *J. Immunol.* **171**, 4969–4973 (2003). doi: [10.4049/jimmunol.171.10.4969](https://doi.org/10.4049/jimmunol.171.10.4969); pmid: [14607890](https://pubmed.ncbi.nlm.nih.gov/14607890/)
62. X. Yu et al., Neutralizing antibodies derived from the B cells of 1918 influenza pandemic survivors. *Nature* **455**, 532–536 (2008). doi: [10.1038/nature07231](https://doi.org/10.1038/nature07231); pmid: [18716625](https://pubmed.ncbi.nlm.nih.gov/18716625/)
63. J. Zuo et al., Robust SARS-CoV-2-specific T-cell immunity is maintained at 6 months following primary infection. *bioRxiv* 2020.11.01.362319 [Preprint]. doi: [10.1101/2020.11.01.362319](https://doi.org/10.1101/2020.11.01.362319)
64. E. Hammarlund et al., Duration of antiviral immunity after smallpox vaccination. *Nat. Med.* **9**, 1131–1137 (2003). doi: [10.1038/nm917](https://doi.org/10.1038/nm917); pmid: [14592586](https://pubmed.ncbi.nlm.nih.gov/14592586/)
65. N. Le Bert et al., SARS-CoV-2-specific T cell immunity in cases of COVID-19 and SARS, and uninfected controls. *Nature* **584**, 457–462 (2020). doi: [10.1038/s41586-020-2550-z](https://doi.org/10.1038/s41586-020-2550-z); pmid: [32668444](https://pubmed.ncbi.nlm.nih.gov/32668444/)
66. N. B. Mercado et al., Single-shot Ad26 vaccine protects against SARS-CoV-2 in rhesus macaques. *Nature* **586**, 583–588 (2020). doi: [10.1038/s41586-020-2607-z](https://doi.org/10.1038/s41586-020-2607-z); pmid: [32731257](https://pubmed.ncbi.nlm.nih.gov/32731257/)
67. K. S. Corbett et al., Evaluation of the mRNA-1273 Vaccine against SARS-CoV-2 in Nonhuman Primates. *N. Engl. J. Med.* **383**, 1544–1555 (2020). doi: [10.1056/NEJMoa2024671](https://doi.org/10.1056/NEJMoa2024671); pmid: [32722908](https://pubmed.ncbi.nlm.nih.gov/32722908/)
68. L. Corey, J. R. Mascola, A. S. Fauci, F. S. Collins, A strategic approach to COVID-19 vaccine R&D. *Science* **368**, 948–950 (2020). doi: [10.1126/science.abc5312](https://doi.org/10.1126/science.abc5312); pmid: [32393526](https://pubmed.ncbi.nlm.nih.gov/32393526/)
69. J. Zhao et al., Airway Memory CD4<sup>+</sup> T Cells Mediate Protective Immunity against Emerging Respiratory Coronaviruses. *Immunity* **44**, 1379–1391 (2016). doi: [10.1016/j.jimmuni.2016.05.006](https://doi.org/10.1016/j.jimmuni.2016.05.006); pmid: [27287409](https://pubmed.ncbi.nlm.nih.gov/27287409/)
70. W. E. Purtha, T. F. Tedder, S. Johnson, D. Bhattacharya, M. S. Diamond, Memory B cells, but not long-lived plasma cells, possess antigen specificities for viral escape mutants. *J. Exp. Med.* **208**, 2599–2606 (2011). doi: [10.1084/jem.20101740](https://doi.org/10.1084/jem.20101740); pmid: [22162833](https://pubmed.ncbi.nlm.nih.gov/22162833/)
71. D. Masopust, A. G. Soerens, Tissue-Resident T Cells and Other Resident Leukocytes. *Annu. Rev. Immunol.* **37**, 521–546 (2019). doi: [10.1146/annurev-immunol-042617-053214](https://doi.org/10.1146/annurev-immunol-042617-053214); pmid: [30726153](https://pubmed.ncbi.nlm.nih.gov/30726153/)
72. H. C. Whittle et al., Effect of subclinical infection on maintaining immunity against measles in vaccinated children in West Africa. *Lancet* **353**, 98–102 (1999). doi: [10.1016/S0140-6736\(98\)02364-2](https://doi.org/10.1016/S0140-6736(98)02364-2); pmid: [10023894](https://pubmed.ncbi.nlm.nih.gov/10023894/)
73. S. A. Plotkin, Vaccines: Correlates of vaccine-induced immunity. *Clin. Infect. Dis.* **47**, 401–409 (2008). doi: [10.1086/589862](https://doi.org/10.1086/589862); pmid: [18558875](https://pubmed.ncbi.nlm.nih.gov/18558875/)
74. N. Burdin, L. K. Handy, S. A. Plotkin, What Is Wrong with Pertussis Vaccine Immunity? The Problem of Waning Effectiveness of Pertussis Vaccines. *Cold Spring Harb. Perspect. Biol.* **9**, a029454 (2017). doi: [10.1101/cshperspect.a029454](https://doi.org/10.1101/cshperspect.a029454); pmid: [28289064](https://pubmed.ncbi.nlm.nih.gov/28289064/)
75. N. van Doremel et al., ChAdOx1 nCoV-19 vaccine prevents SARS-CoV-2 pneumonia in rhesus macaques. *Nature* **586**, 578–582 (2020). doi: [10.1038/s41586-020-2608-y](https://doi.org/10.1038/s41586-020-2608-y); pmid: [32731258](https://pubmed.ncbi.nlm.nih.gov/32731258/)
76. R. L. Tillet et al., Genomic evidence for reinfection with SARS-CoV-2: A case study. *Lancet Infect. Dis.* **21**, 52–58 (2021). doi: [10.1016/S1473-3099\(20\)30764-7](https://doi.org/10.1016/S1473-3099(20)30764-7); pmid: [33058797](https://pubmed.ncbi.nlm.nih.gov/33058797/)
77. K. K.-W. To et al., COVID-19 re-infection by a phylogenetically distinct SARS-coronavirus-2 strain confirmed by whole genome sequencing. *Clin. Infect. Dis.* **ciaa1275**; pmid: [32840608](https://pubmed.ncbi.nlm.nih.gov/32840608/)
78. D. Wyllie et al., SARS-CoV-2 responsive T cell numbers are associated with protection from COVID-19: A prospective cohort study in keyworkers. *medRxiv* 2020.11.02.20222778 [Preprint]. 4 November 2020. doi: [10.1101/2020.11.02.20222778](https://doi.org/10.1101/2020.11.02.20222778)
79. S. F. Lumley et al., Antibodies to SARS-CoV-2 are associated with protection against reinfection. *medRxiv* 2020.11.18.20234369 [Preprint]. 19 November 2020. doi: [10.1101/2020.11.18.20234369](https://doi.org/10.1101/2020.11.18.20234369)
80. J. H. Beigel et al., Remdesivir for the Treatment of Covid-19 - Final Report. *N. Engl. J. Med.* **383**, 1813–1826 (2020). doi: [10.1056/NEJMoa2007764](https://doi.org/10.1056/NEJMoa2007764); pmid: [32445440](https://pubmed.ncbi.nlm.nih.gov/32445440/)
81. D. Wrapp et al., Cryo-EM structure of the 2019-nCoV spike in the prefusion conformation. *Science* **367**, 1260–1263 (2020). doi: [10.1126/science.abb2507](https://doi.org/10.1126/science.abb2507); pmid: [32075877](https://pubmed.ncbi.nlm.nih.gov/32075877/)
82. F. Amanat et al., A serological assay to detect SARS-CoV-2 seroconversion in humans. *Nat. Med.* **26**, 1033–1036 (2020). doi: [10.1038/s41591-020-0913-5](https://doi.org/10.1038/s41591-020-0913-5); pmid: [32398876](https://pubmed.ncbi.nlm.nih.gov/32398876/)
83. J. Mestecky et al., Evaluation of monoclonal antibodies with specificity for human IgA, IgG subclasses and allotypes and secretory component. Results of an IUIS/WHO collaborative study. *J. Immunol. Methods* **193**, 103–148 (1996). doi: [10.1016/0022-1759\(95\)00289-8](https://doi.org/10.1016/0022-1759(95)00289-8); pmid: [8699027](https://pubmed.ncbi.nlm.nih.gov/8699027/)
84. GraphPad, GraphPad Prism 8 Curve Fitting Guide (2020); [www.graphpad.com/guides/prism/8/curve-fitting/index.htm](http://www.graphpad.com/guides/prism/8/curve-fitting/index.htm).

**ACKNOWLEDGMENTS**

We thank the LJI Clinical Core, specifically G. Levi and B. Schwan for healthy donor enrollment and blood sample procurement. We thank C. Moderbacher for input on data analysis. We are also grateful to the Mt. Sinai Personalized Virology Initiative for sharing banked samples from study participants with COVID-19. We are grateful to A. Wajnberg for study participant referrals and to the Personalized Virology Initiative (G. Kleiner, L. C. F. Mulder, M. Saksema, K. Srivastava, C. Gleason, C. M. Bermúdez-González, K. Beach, K. Russo, L. Sominsky, E. Ferreri, R. Chernet, L. Eaker, A. Salimbangon, D. Jurczyszak, H. Alshammary, W. Mendez, A. Amoako, S. Fabre, S. Suthakaran, M. Awawda, E. Hirsch, A. Shin) for sharing banked samples from study participants with COVID-19. **Funding:** This work was funded by the NIH NIAID under awards AI142742 (Cooperative Centers for Human Immunology) (A.S., S.C.), NIH contract no. 75N9301900065 (D.W., A.S.), U01 AI14995-03 (A.S., P.B.), and U01 CA260541-01 (D.W.). This work

was additionally supported in part by LJI Institutional Funds, the John and Mary Tu Foundation (D.S.), the NIAID under K08 award AI135078 (J.M.D.), UCSD T32s AI007036 and AI007384 Infectious Diseases Division (S.I.R., S.A.R.), and the Bill and Melinda Gates Foundation INV-006133 from the Therapeutics Accelerator, Mastercard, Wellcome, private philanthropic contributions (K.M.H., E.O.S., S.C.), and a FastGrant from Emergent Ventures in aid of COVID-19 research. This work was partially supported by the NIAID Centers of Excellence for Influenza Research and Surveillance (CEIRS) contract HHSN272201400008C (F.K., for reagent generation), the Collaborative Influenza Vaccine Innovation Centers (CIVIC) contract 75N93019C00051, the JPB foundation (F.K., V.S.), the Cohen Foundation (V.S., F.K.), and the Open Philanthropy Project (no. 2020-21561; F.K., V.S.), as well as by other philanthropic donations. We also thank all of the COVID-19 and healthy human subjects who made this research possible through their generous blood donations. **Author contributions:**

Conceptualization, S.C., A.S., and D.W.; Investigation, J.M.D., J.M., Y.K., K.M.H., E.D.Y., C.E.F., A.G., S.H., and C.N.; Formal Analysis, J.M.D., J.M., Y.K., K.M.H., C.E.F., S.H., B.P., D.W., A.S., and

S.C.; Patient Recruitment and Samples, S.I.R., A.F., S.A.R., F.K., V.S., D.M.S., and D.W.; Material Resources, F.K., V.S., V.R., E.O.S., D.W., A.S., and S.C.; Data Curation, Y.K., J.M.D., J.M., and S.H.; Writing, Y.K., J.M.D., J.M., S.I.R., D.W., A.S., and S.C.; Supervision, D.W., A.S., and S.C.; Project Administration, A.F. **Competing interests:** A.S. is a consultant for Gritstone, Flow Pharma, Merck, Epitogenesis, Gilead, and Avalia. S.C. is a consultant for Avalia. L.J.I. has filed for patent protection for various aspects of T cell epitope and vaccine design work. Mount Sinai has licensed serological assays to commercial entities and has filed for patent protection for serological assays. D.S., F.A., V.S., and F.K. are listed as inventors on the pending patent application (F.K., V.S.) and Newcastle disease virus (NDV)-based SARS-CoV-2 vaccines that name F.K. as inventor. All other authors declare no conflict of interest. **Data and materials availability:** All data are provided in the supplementary materials. Epitope pools used in this paper will be made available to the scientific community upon request and execution of a material transfer agreement. This work is licensed under a Creative Commons Attribution 4.0 International (CC BY 4.0) license, which permits unrestricted

use, distribution, and reproduction in any medium, provided the original work is properly cited. To view a copy of this license, visit <https://creativecommons.org/licenses/by/4.0/>. This license does not apply to figures/photos/artwork or other content included in the article that is credited to a third party; obtain authorization from the rights holder before using such material.

## SUPPLEMENTARY MATERIALS

[science.sciencemag.org/content/371/6529/eabf4063/suppl/DC1](https://science.sciencemag.org/content/371/6529/eabf4063/suppl/DC1)

Figs. S1 to S10

Tables S1 and S2

MDAR Reproducibility Checklist

Data File S1

[View/request a protocol for this paper from Bio-protocol.](#)

23 October 2020; accepted 23 December 2020

Published online 6 January 2021

10.1126/science.abf4063

## Immunological memory to SARS-CoV-2 assessed for up to 8 months after infection

Jennifer M. Dan, Jose Mateus, Yu Kato, Kathryn M. Hastie, Esther Dawen Yu, Caterina E. Faliti, Alba Grifoni, Sydney I. Ramirez, Sonya Haupt, April Frazier, Catherine Nakao, Vamseedhar Rayaprolu, Stephen A. Rawlings, Bjoern Peters, Florian Krammer, Viviana Simon, Erica Ollmann Saphire, Davey M. Smith, Daniela Weiskopf, Alessandro Sette and Shane Crotty

Science 371 (6529), eabf4063.  
DOI: 10.1126/science.abf4063 originally published online January 6, 2021

### Variable memory

Immune memory against severe acute respiratory syndrome coronavirus 2 (SARS-CoV-2) helps to determine protection against reinfection, disease risk, and vaccine efficacy. Using 188 human cases across the range of severity of COVID-19, Dan *et al.* analyzed cross-sectional data describing the dynamics of SARS-CoV-2 memory B cells, CD8<sup>+</sup> T cells, and CD4<sup>+</sup> T cells for more than 6 months after infection. The authors found a high degree of heterogeneity in the magnitude of adaptive immune responses that persisted into the immune memory phase to the virus. However, immune memory in three immunological compartments remained measurable in greater than 90% of subjects for more than 5 months after infection. Despite the heterogeneity of immune responses, these results show that durable immunity against secondary COVID-19 disease is a possibility for most individuals.

Science, this issue p. eabf4063

### ARTICLE TOOLS

<http://science.sciencemag.org/content/371/6529/eabf4063>

### SUPPLEMENTARY MATERIALS

<http://science.sciencemag.org/content/suppl/2021/01/05/science.abf4063.DC1>

### RELATED CONTENT

<http://stm.sciencemag.org/content/scitransmed/13/577/eabd2223.full>  
<http://stm.sciencemag.org/content/scitransmed/12/564/eabd5487.full>  
<http://stm.sciencemag.org/content/scitransmed/13/578/eabd6990.full>  
<http://stm.sciencemag.org/content/scitransmed/13/577/eabf1555.full>  
<http://stke.sciencemag.org/content/sigtrans/14/673/eabc5763.full>

### REFERENCES

This article cites 81 articles, 30 of which you can access for free  
<http://science.sciencemag.org/content/371/6529/eabf4063#BIBL>

### PERMISSIONS

<http://www.sciencemag.org/help/reprints-and-permissions>

Use of this article is subject to the [Terms of Service](#)

---

Science (print ISSN 0036-8075; online ISSN 1095-9203) is published by the American Association for the Advancement of Science, 1200 New York Avenue NW, Washington, DC 20005. The title *Science* is a registered trademark of AAAS.

Copyright © 2021 The Authors, some rights reserved; exclusive licensee American Association for the Advancement of Science. No claim to original U.S. Government Works